scientific reports

Check for updates

OPEN

Thermal behavior of the Klein Gordon oscillator in a dynamical noncommutative space

Ilyas Haouam

We investigate the thermal properties of the Klein–Gordon oscillator in a dynamical noncommutative space. These properties are determined via the partition function, which is derived using the Euler–Maclaurin formula. Analytical expressions for the partition function, free energy, internal energy, entropy, and specific heat capacity of the deformed system are obtained and numerically evaluated. The distinct roles of dynamical and flat noncommutative spaces in modulating these properties are rigorously examined and compared. Furthermore, visual representations are provided to illustrate the influence of the deformations on the system's thermal behavior. The findings highlight significant deviations in thermal behavior induced by noncommutativity, underscoring its profound physical implications.

Keywords Position-dependent noncommutative space, Dynamical noncommutative space, Klein-Gordon oscillator, Euler-MacLaurin Formula, Thermal properties

In recent decades, there has been growing interest in understanding the thermodynamic and magnetic properties of quantum systems under various potential fields, within both non-relativistic and relativistic regimes. To explore such phenomena, simplified yet powerful models such as the Klein–Gordon (KG), Dirac, DKP, Pauli, and harmonic oscillators are often employed as foundational tools in theoretical research. These models mainly differ in how they incorporate relativistic effects and the spin characteristics of the particles they describe. In this work, we focus on the thermal characteristics of the KG oscillator within a dynamical noncommutative (DNC) space. This study lies at the intersection of relativistic quantum mechanics, statistical physics, and noncommutative (NC) geometry, intertwining three advanced concepts: the KG oscillator, NC geometry, and thermal functions.

Originating from the relativistic KG equation, the KG oscillator incorporates a harmonic oscillator potential into the dynamics of spin-0 particles, as introduced by Bruce & Minning[1,2]. In its relativistic formulation, it reduces to the well-known non-relativistic harmonic oscillator under suitable limits, yet it also exhibits novel features, such as modified energy spectra and symmetry properties. Since its introduction, the KG oscillator has attracted considerable interest, and has been extensively studied in diverse scenarios and settings, including NC, anti-de Sitter, topologically nontrivial, and cosmic string space-time, as well as with Kaluza–Klein theory, minimal length, rainbow gravity[3–14]. Recent studies have further expanded its exploration in relativistic and cosmological contexts. For instance[15], investigates the KG oscillator within a cosmological space-time characterized by a cosmological constant[16]. explores the quantum dynamics of scalar particles governed by the KG equation under rainbow gravity effects in the Bonnor–Melvin-Lambda background[17]. analyzes the relativistic quantum behavior of spin-zero particles and antiparticles (scalar fields) in a magnetic Bonnor–Melvin–Lambda universe[18]. studies a position-dependent mass relativistic quantum oscillator within an Einstein–Maxwell–Lambda space-time, employing a modified KG equation to analyze position-dependent mass oscillator fields. Moreover, extensive research has delved into the alignment between the KG oscillator and thermodynamical aspects. For instance, studies have explored the solutions of the D-dimensional KG oscillator and its thermodynamic properties within the Snyder-de Sitter algebra[19], as well as the exact solutions to the 2D KG oscillator in a NC complex phase-space and its thermal properties[20]. Additionally, investigations have been conducted on the thermal properties of the 2D KG oscillator in a cosmic string spacetime using the Poisson approximation[21], and the statistical properties of the KG oscillator in NC space[22]. Furthermore, research has examined the partition function and mean energy of the 3D KG oscillator in a background magnetic field within NC space[23].

NC geometry has emerged as a prominent area of study, capturing considerable attention in high-energy and contemporary physics, including quantum physics[24,25], quantum field theory[26,27], Standard Model[28], string theories[29], matrix theory[30], black holes, gravity, and cosmology[31,32]. Studies have underscored the importance of

Laboratoire de Physique Mathématique et de Physique Subatomique (LPMPS), Université Frères Mentouri, Constantine 25000, Algeria. email: ilyashaouam@live.fr; ilyas.haouam@tmp.umc.edu.dz

NC spaces in understanding phenomena occurring at extremely short distances and within high-energy ranges. Various types of NC spaces have been explored, such as complex[33] and time-dependent NC[20] spaces, etc[14,20,33–35]. Among these, a specific type known as position-dependent NC space, or DNC space, is particularly significant to our study. In this context, the NC parameter Θ is treated as a function of coordinates, i.e., $\Theta \to \Theta(X, Y)$. The transition from the commutative setting to the NC one (or vice versa) is accomplished using several substantial techniques, as has been extensively discussed in the literature, including: (i) Weyl–Wigner maps[36], employing the Weyl operators. (ii) Moyal–Weyl product, or $\star$product, instead of ordinary product[37,38]. (iii) Bopp-shift transformations[39,40]. (iv) Seiberg–Witten maps[24]. In our present study, we adopt the Bopp-shift method to facilitate this transition.

In this study, we investigate the effects of both the DNC and flat NC spaces on the thermal properties of the KG oscillator via the partition function, employing the Euler-Maclaurin formula, including free energy, internal energy, entropy, and specific heat capacity. This work is part of a broader investigation into the NC spaces subject, aiming to shed more light on the phenomenological implications of them. It builds upon our previous research exploring the interplay between DNC space and relativistic quantum mechanics. As examples, we mention[14], where we investigated the effects of the DNC space on the relativistic and nonrelativistic 2D KG oscillators in the framework of the perturbation theory. Additionally, in[41], we have addressed the eigensystems of the 2D DNC Dirac oscillator; furthermore, we mention[42], where we have investigated the graphene in the framework of DNC spaces and delve into some of its thermodynamic quantities at zero temperature limit and extreme relativistic case. Likewise[43], that aims to investigate the Landau problem in the framework of a DNC space and its magnetoconductivity by employing the Kubo formula. It is also important to mention limitations of our work. It is also important to highlight the limitations of the present work. This study is restricted to the 2D KG oscillator model and does not consider interactions with external magnetic fields. The analysis assumes a specific form of position-dependent noncommutativity and does not incorporate higher-order deformation corrections. Moreover, the partition function is derived using the Euler–Maclaurin approximation, which may reduce accuracy at very low temperatures. Finally, although non-Hermitian features inherent in the DNC framework are acknowledged, their consequences for thermodynamic consistency and physical observables remain unexplored and represent a promising direction for future research.

The rest of the paper is outlined as follows. In Sec. 2, the system of the KG oscillator within DNC space is briefly reviewed. Sub-Sec. 2.1 provides a concise overview of the DNC formalism, while sub-Sec. 2.2 revisits the the 2D KG oscillator in DNC space. Sec. 3 extensively investigates the thermal properties of the DNC KG oscillator. Sub-Sec. 3.1 presents the methods and numerical results, and sub-Secs. 3.2 provides graphical analyses and discussions. Finally, Sec. 4 concludes the paper.

KG oscillator system within DNC space

In this section, we present the DNC formalism used in this work. Additionally, we revisit the 2D KG oscillator and its solutions within the DNC space.

Brief aspects of the DNC formalism

Let briefly review the fundamental equations of the DNC space algebra employed in this study. At the string scale, extremely small scale, space acquires a NC structure, and the position coordinates no longer commute[24]. As a consequence, the canonical variables satisfy a modified Heisenberg commutation relation in the 2D flat NC space, expressed as

$$\left[x_i^{nc}, x_j^{nc}\right] = \mathrm{i}\Theta_{ij} = \mathrm{i}\Theta\epsilon_{ij}, \tag{1}$$

where ϵ_{ij} is the Levi-Civita symbol. In the simplest scenario, the NC parameter Θ is typically treated as a fixed real constant. However, in a more general framework, Θ may depend on spatial coordinates[43] or even on time[44]. In this study, we consider a position-dependent NC space, commonly referred to as DNC space, following the approach of[14,34], where position-dependent properties are incorporated by introducing a set of 2D non-Hermitian variables X, Y, P_X, and P_Y. Within this framework, Θ is treated as a function of the coordinates, given by

$$\Theta\left(X, Y\right) = \Theta\left(1 + \tau Y^2\right), \tag{2}$$

where τ is the DNC parameter, also known as the non-Hermitian parameter[45]. Many other forms for $\Theta\left(X, Y\right)$ have indeed been proposed in the literature. For example, in[46] one finds $\Theta\left(X, Y\right) = \Theta\left(1 - \tau Y + \tau Y^2\right)$, while in[35] the form is given by $\Theta\left(X, Y\right) = \Theta\left[1 + \Theta\alpha\left(1 + X^2 + Y^2\right)\right]^{-1}$ with α is a locality parameter. However, the resulting coordinates are non-Hermitian. As noted in[47], these deformed structures are intrinsically linked to non-Hermitian Hamiltonian systems[48]. The following explanation outlines the approach taken to address this issue. In the DNC space, or τ-deformed space, the non-Hermitian operators satisfy the following relations[34]:

$$\begin{aligned}
&[X, Y] = i\Theta\left(1 + \tau Y^2\right), \\
&[X, P_y] = 2i\tau Y\left(\Theta P_y + \hbar X\right), \\
&[X, P_x] = [Y, P_y] = i\hbar\left(1 + \tau Y^2\right), \\
&[Y, P_x] = [P_x, P_y] = 0.
\end{aligned} \tag{3}$$

In the DNC phase-space, instead of a vanishing commutator between P_x, P_y, as in Eq. (3), we have $[P_x, P_y] = i\bar{\Theta}\left(1+\tau Y^2\right)$, where $\bar{\Theta}$ is a constant NC parameter associated with momentum, having the dimension $\mathrm{M}^2\mathrm{L}^2\mathrm{T}^{-1}$. It is worth noting that Θ and τ have dimensions of L^2 and L^{-2}, respectively.

The algebra in (3) can be expressed in terms of the standard Hermitian flat NC variable operators x^{nc}, y^{nc}, p_x^{nc}, and p_y^{nc} as follows:

$$X = \left(1+\tau\left(y^{nc}\right)^2\right)x^{nc},\ Y = y^{nc},\ P_x = p_x^{nc},\ \text{and}\ P_y = \left(1+\tau\left(y^{nc}\right)^2\right)p_y^{nc}. \tag{4}$$

As $\tau \to 0$, the following non-DNC (or flat NC) commutation relations are recovered:

$$\begin{array}{l} \left[x^{nc}, y^{nc}\right] = i\Theta, \\ \left[x^{nc}, p_x^{nc}\right] = \left[y^{nc}, p_y^{nc}\right] = i\hbar, \\ \left[x^{nc}, p_y^{nc}\right] = \left[y^{nc}, p_x^{nc}\right] = \left[p_x^{nc}, p_y^{nc}\right] = 0. \end{array} \tag{5}$$

As previously mentioned, the representation in (4), reveals that some of the involved operators are non-Hermitian. Specifically, we have

$$X^\dagger = X + 2i\tau\Theta Y, \quad Y^\dagger = Y, \quad P_x^\dagger = P_x \text{ and } \quad P_y^\dagger = P_y - 2i\tau\hbar Y. \tag{6}$$

This clearly indicates that the operators X and P_y are non-Hermitian. As a result, the Hamiltonian, which includes these operators, will generally also not be Hermitian, i.e., $\mathscr{H}^\dagger\left(X_i, P_i\right) \neq \mathscr{H}\left(X_i, P_i\right)$. To address this issue, the non-Hermitian variables are transformed into Hermitian ones using the Dyson map[34] $\kappa = \left(1+\tau Y^2\right)^{-\frac{1}{2}}$ applied to non-Hermitian observables $O \neq O^\dagger$ ensuring that the adjoint of these operators is given by $O^\dagger \xrightarrow{\kappa} \kappa O \kappa^{-1} = \mathcal{O} = \mathcal{O}^\dagger$. We require $\tau \geq 0$ to ensure that the Dyson map remains non-singular. Consequently, the new Hermitian variables $\mathcal{X}$, $\mathcal{Y}$, $\mathcal{P}_x$, and $\mathcal{P}_y$ are represented in terms of flat NC variables as follows:

$$\begin{array}{l} \mathcal{X} = \kappa X \kappa^{-1} = \left(1+\tau\left(y^{nc}\right)^2\right)^{\frac{1}{2}} x^{nc} \left(1+\tau\left(y^{nc}\right)^2\right)^{\frac{1}{2}} = \mathcal{X}^\dagger, \\ \mathcal{Y} = \kappa Y \kappa^{-1} = y^{nc} = \mathcal{Y}^\dagger, \\ \mathcal{P}_x = \kappa P_x \kappa^{-1} = p_x^{nc} = \mathcal{P}_x^\dagger, \\ \mathcal{P}_y = \kappa P_y \kappa^{-1} = \left(1+\tau\left(y^{nc}\right)^2\right)^{\frac{1}{2}} p_y^{nc} \left(1+\tau\left(y^{nc}\right)^2\right)^{\frac{1}{2}} = \mathcal{P}_y^\dagger. \end{array} \tag{7}$$

The new Hermitian DNC variables (7) obey the following commutation relations:

$$\begin{array}{l} \left[\mathcal{X}, \mathcal{Y}\right] = i\Theta\left(1+\tau\mathcal{Y}^2\right), \\ \left[\mathcal{X}, \mathcal{P}_x\right] = \left[\mathcal{Y}, \mathcal{P}_y\right] = i\hbar\left(1+\tau\mathcal{Y}^2\right), \\ \left[\mathcal{X}, \mathcal{P}_y\right] = 2i\tau\mathcal{Y}\left(\Theta\mathcal{P}_y + \hbar\mathcal{X}\right), \\ \left[\mathcal{Y}, \mathcal{P}_x\right] = 0,\ \left[\mathcal{P}_x, \mathcal{P}_y\right] = 0. \end{array} \tag{8}$$

Using the Bopp-shift, the flat NC variables can be mapped to the standard commutative variables as follows[39,40]:

$$x^{nc} = x - \tfrac{\Theta}{2\hbar}p_y \quad y^{nc} = y + \tfrac{\Theta}{2\hbar}p_x, \quad p_x^{nc} = p_x, \text{ and } \quad p_y^{nc} = p_y. \tag{9}$$

In the DNC space (for a system of variables satisfying Eq. (3)), the uncertainty relations is giving by $\triangle\mathscr{A}\triangle\mathscr{B} \geq \frac{1}{2}\left|\langle[\mathscr{A}, \mathscr{B}]\rangle_\rho\right|$ where $\mathscr{A}, \mathscr{B} \in \{X, Y, P_X, P_Y\}$. Hence, there is a minimum length associated with the coordinate X in a simultaneous measurement of X, Y[34]:

$$\triangle X_{\min} = \Theta\sqrt{\tau}\sqrt{1+\tau\langle Y\rangle_\rho^2}, \tag{10}$$

while there is no minimum length for Y. Knowing that $\rho = \kappa^2 = 1/(1+\tau Y^2)$ represents the metric operator, which is Hermitian, and $\langle Y\rangle_\rho$ is the expectation value of Y with respect to this metric. This is given by

$$\langle Y\rangle_\rho = \langle\Psi| Y |\Psi\rangle_\rho. \tag{11}$$

The inner product, expressed in terms of the standard inner product, is defined as

$$\langle\Phi \mid \Psi\rangle_\rho := \langle\Phi \mid \rho\Psi\rangle = \int_{-\infty}^{+\infty} \frac{dy}{1+\tau y^2}\Psi^*(y)\,\Phi(y), \tag{12}$$

for arbitrary states $\langle\Phi|$ and $|\Psi\rangle$. Subsequently, any observable operator $\mathscr{P}$ must satisfy $\langle\Phi \mid \mathscr{P}\Psi\rangle_\rho = \langle\mathscr{P}\Phi \mid \Psi\rangle_\rho$, which makes $\mathscr{P}$ Hermitian with respect to this metric. Note that the uncertainty relation for the non-Hermitians position operators X, Y, under Eq. (12), we have $\triangle X\triangle Y \geq \frac{1}{2}\left|i\Theta\left\langle 1+\tau Y^2\right\rangle\right|$.

Additionally, we find a minimal momentum in a simultaneous Y, P_y measurement[34]:

$$\triangle\left(P_y\right)_{\min} = \hbar\sqrt{\tau}\sqrt{1+\tau\langle Y\rangle_\rho^2}, \tag{13}$$

while we do not encounter any minimal length or minimal momentum in a simultaneous X, P_x measurement. Note that the solutions of simultaneous measurements of Y, P_y are given

$$\triangle Y = \frac{1}{\hbar\tau}\triangle P_y \pm \frac{1}{\hbar\tau}\sqrt{\triangle P_y^2 - \hbar^2\tau\left(1+\tau\left\langle Y\right\rangle^2\right)}. \tag{14}$$

A key physical implication and motivation for position-dependent noncommutativity is that objects in 2D space exhibit string-like behavior[14,34,42]. In particular, within this framework, a minimum length for X exists in a simultaneous measurement of X and Y, beyond which further resolution is unattainable. This implies that objects in the 2D space defined by X and Y, inherently are of string-like type naturally. As a result, DNC space reveals a deeper and more fundamental connection to string theory than the flat NC space. Furthermore, investigating the dynamics of the KG oscillator system within the DNC space not only offers insights into the interplay between DNC space and non-Hermitian Hamiltonians but also may advances our understanding of its link to string theory. Such studies may drive new theoretical developments, substantial advancements, and meaningful phenomenological implications that extend well beyond the ordinary NC framework.

Review on the 2D KG oscillator in DNC space

The KG oscillator in 2D commutative space is given by the following equation[1]:

$$\left\{c^2\left(p_x+im\omega x\right)\left(p_x-im\omega x\right)+c^2\left(p_y+im\omega y\right)\left(p_y-im\omega y\right)+\left(mc^2\right)^2-E_{n,l}^2\right\}\psi_{n,l}\left(\overrightarrow{r}\right)=0, \tag{15}$$

where ω is the oscillator angular frequency, m is the rest mass of the scalar particle. In the DNC space, we substitute Eq. (7) and (9) in Eq. (15) obtaining[14]:

$$\begin{aligned} &c^2\left\{p_x^2+p_y^2+m^2\omega^2\left(x^2+y^2\right)-2m\hbar\omega-\tfrac{m^2\omega^2}{\hbar}L_z\Theta\right\}\left|\psi_{n,l}\right\rangle+\tau c^2\left(\tfrac{p_y^2y^2+y^2p_y^2}{2}\right.\\ &\left.+p_yy^2p_y+2m^2\omega^2x^2y^2\right)\left|\psi_{n,l}\right\rangle+\left\{\left(mc^2\right)^2-\left(E_{n,l}^{\mathrm{DNC}}\right)^2\right\}\left|\psi_{n,l}\right\rangle+\mathcal{O}\left(\tau\Theta,\Theta^2,\tau^2\right)=0. \end{aligned} \tag{16}$$

where the wave function of the system in question is

$$\left|\psi_{n,l}\right\rangle = \left|\frac{n+l}{2},\frac{n-l}{2}\right>. \tag{17}$$

The energy levels of the DNC KG oscillator (16), including first-order correction is given by[14]:

$$E_{n,l}^{\mathrm{DNC}} = E_{n,l}^{\pm}\left(\Theta,\tau\right) = \pm mc^2\sqrt{2\mathscr{A}\left(n+1\right)-2\mathscr{A}-\frac{\mathscr{A}^2}{\mathscr{B}}\Theta l+\mathscr{B}\tau+1}, \tag{18}$$

with $\mathscr{A}=\frac{\hbar\omega}{mc^2}$ is a parameter that controls the nonrelativistic limit, and $\mathscr{B}=\frac{\hbar^2}{m^2c^2}$. Note that The appearance of the deformation parameters in the energy spectrum lifts the degeneracy of the energy levels. By setting $\tau=0$, we recover the result of the flat NC space, similar to that obtained in[3] with $l=m_l$, giving by

$$E_{n,l}^{\mathrm{NC}} = E_{n,l}^{\pm}\left(\Theta\right) = \pm\sqrt{2\hbar\omega mc^2\left(n+1\right)-\omega^2m^2c^2\Theta l+m^2c^4-2mc^2\hbar\omega}, \tag{19}$$

which resembles the behavior seen in the Zeeman effect. Furthermore, by setting $\tau=\Theta=0$, we retrieve the well-known results corresponding to commutative space.

Thermal properties of the DNC KG oscillator

Methods and numerical results

In this part, we investigate the effect of DNC and flat NC spaces on the thermal properties of the KG oscillator. So, in the framework of statistical physics, these properties are determined using the partition function $Z\left(\beta\right)$. Therefore, we first compute the partition function for the deformed KG oscillator by summing over all possible energy levels of the system (single oscillator) as follows:

$$Z\left(\beta\right)=\sum_{n=0}^{\infty}\mathrm{e}^{-\beta\left(E_n-E_0\right)}\ \text{with}\ \beta=\frac{1}{K_BT}, \tag{20}$$

where β is the Boltzmann factor, E_0 represents the ground-state energy corresponding to $n=0$, T denotes the absolute temperature, and K_B is the Boltzmann constant. Revisiting the spectrum in Eq. (18), it can be expressed as follows:

$$E_n^{\pm}=\pm mc^2\sqrt{\mu n+\lambda}, \tag{21}$$

with

$$\mu = 2\mathscr{A}, \text{and } \lambda = 1 - \frac{\mathscr{A}^2}{\mathscr{B}}\Theta l + \mathscr{B}\tau. \tag{22}$$

Here, we restrict our analysis to the stationary state's positive energy solutions, as the partition function fails to converge with the inclusion of negative energy solutions in the canonical ensemble. It is also important to note that the KG oscillator admits an exact Foldy–Wouthuysen transformation, which ensures that positive and negative energy solutions do not mix. This transformation diagonalizes the system's Hamiltonian into separate blocks corresponding to particles (positive energy) and antiparticles (negative energy), resulting in two decoupled equations. Consequently, the time evolution of each component is independent, with no transitions between positive- and negative-energy states. This separation ensures a consistent particle–antiparticle interpretation, with a conserved and positive-definite probability current in the positive-energy sector. As a result, thermodynamic properties can be studied without concern for spurious particle-antiparticle mixing. Therefore, in this work, we consider only the positive energy states to contribute to the thermodynamic properties of the KG oscillator. Now, based on the form of the energy eigenvalues (21) the single-oscillator partition function is written as

$$Z(\beta) = \sum_{n=0}^{\infty} \mathrm{e}^{-\beta mc^2\left(\sqrt{\mu n+\lambda}-\sqrt{\lambda}\right)} = \mathrm{e}^{\frac{\sqrt{\lambda}}{\kappa}} \sum_{n=0}^{\infty} \mathrm{e}^{-\frac{1}{\kappa}\sqrt{\mu n+\lambda}}, \tag{23}$$

with $\kappa = \frac{1}{\beta mc^2} = \frac{T}{T_0}$. Knowing that $T_0 = \frac{mc^2}{K_B} \approx 5.93 \times 10^{9}\mathrm{K}$ is the characteristic temperature (its nature is very similar to the Debay temperature) that divides the range of temperature to very high temperature, $T \gg T_0$, and very low temperature, $T \ll T_0$ regions[49]. To evaluate the partition function, we apply the Euler-Maclaurin formula. However, let us first test the convergence of the partition function (23) through the integral of the function $f(x) = \exp\left(-\frac{1}{\kappa}\sqrt{\mu x+\lambda}\right)$, which is a monotonically decreasing function

$$I(\kappa) = \int_0^{+\infty} \mathrm{e}^{-\frac{1}{\kappa}\sqrt{\mu x+\lambda}} dx = \frac{2\kappa^2}{\mu}\left(1+\frac{1}{\kappa}\sqrt{\lambda}\right)\mathrm{e}^{-\frac{\sqrt{\lambda}}{\kappa}}. \tag{24}$$

According to the theorems of convergent series, it follows that the partition function is convergent. Therefore, we apply the Euler-Maclaurin formula[50,51]:

$$\sum_{n=0}^{\infty} f(n) = \frac{1}{2}f(0) + \int_0^{+\infty} f(x)\,dx - \sum_{p=1}^{\infty} \frac{1}{(2p)!} B_{2p} f^{(2p-1)}(0), \tag{25}$$

where $f^{(2p-1)}(0)$ denotes the $(2p-1)$th derivative evaluated at $x = 0$. The coefficients B_{2p} are Bernoulli numbers, defined as[50]

$$B_n = \frac{2(2n)!}{(2\pi)^{2n}} \sum_{p=1}^{\infty} p^{-2n}, \tag{26}$$

with specific values such as $B_2 = 1/6$, $B_4 = -1/30$, and $B_6 = 1/42$... Then, using Eq. (25), one can find the partition function as follows:

$$Z(\kappa) = \frac{1}{2} + \frac{2\kappa^2}{\mu}\left(1+\frac{1}{\kappa}\sqrt{\lambda}\right) - \mathrm{e}^{\frac{\sqrt{\lambda}}{\kappa}} \sum_{p=1}^{\infty} \frac{1}{(2p)!} B_{2p} f^{(2p-1)}(0). \tag{27}$$

Now, To determine the partition function, we need to calculate the sum in Eq. (27). So, up to $p = 2$ this sum can be written as:

$$\mathrm{e}^{\frac{\sqrt{\lambda}}{\kappa}} \sum_{p=1}^{\infty} \frac{1}{(2p)!} B_{2p} f^{(2p-1)}(0) = \frac{1}{24}\frac{\mu}{\kappa\sqrt{\lambda}} - \frac{1}{1920}\frac{\mu^3}{\kappa\lambda^{5/2}} - \frac{1}{1920}\frac{\mu^3}{\kappa^2\lambda^2} - \frac{1}{5760}\frac{\mu^3}{\kappa^3\lambda^{3/2}}. \tag{28}$$

Finally, we find the partition function as follows:

$$Z(\kappa) = \frac{1}{2} + 2\frac{\sqrt{\lambda}}{\mu}\kappa + \frac{2}{\mu}\kappa^2 + \left(\frac{1}{1920}\frac{\mu^3}{\lambda^{5/2}} - \frac{1}{24}\frac{\mu}{\sqrt{\lambda}}\right)\frac{1}{\kappa} + \frac{1}{1920}\frac{\mu^3}{\lambda^2}\frac{1}{\kappa^2} + \frac{1}{5760}\frac{\mu^3}{\lambda^{3/2}}\frac{1}{\kappa^3}. \tag{29}$$

Subsequently, employing Eq. (22), the partition function in DNC space is

$$Z(\kappa,\Theta,\tau)=\frac{1}{2}+\frac{\sqrt{1-\frac{\mathscr{A}^2}{\mathscr{B}}\Theta l+\mathscr{B}\tau}}{\mathscr{A}}\kappa+\frac{1}{\mathscr{A}}\kappa^2+\left(\frac{1}{240}\frac{\mathscr{A}^3}{\left(1-\frac{\mathscr{A}^2}{\mathscr{B}}\Theta l+\mathscr{B}\tau\right)^{5/2}}-\frac{1}{12}\frac{\mathscr{A}}{\sqrt{1-\frac{\mathscr{A}^2}{\mathscr{B}}\Theta l+\mathscr{B}\tau}}\right)\frac{1}{\kappa}$$
$$+\frac{1}{240}\frac{\mathscr{A}^3}{\left(1-\frac{\mathscr{A}^2}{\mathscr{B}}\Theta l+\mathscr{B}\tau\right)^{2}}\frac{1}{\kappa^2}+\frac{1}{720}\frac{\mathscr{A}^3}{\left(1-\frac{\mathscr{A}^2}{\mathscr{B}}\Theta l+\mathscr{B}\tau\right)^{3/2}}\frac{1}{\kappa^3}. \tag{30}$$

According to Eq. (30), we can see that the partition function depends on the DNC and NC parameters. Importantly, only the first three terms significantly influence the calculations at very high temperatures. In contrast, at very low temperatures, terms involving $\frac{1}{\kappa}$, $\frac{1}{\kappa^2}$, and $\frac{1}{\kappa^3}$ dominate the behavior of Z. At moderate temperatures—where neither low nor high extremes prevail—all terms contribute, reflecting a crossover regime between these thermal limits. The DNC KG oscillator partition function can be easily extended to an N-particle system without internal interactions using

$$\mathcal{Z}(\kappa,\Theta,\tau)=Z^N(\kappa,\Theta,\tau). \tag{31}$$

Key thermal properties such as free energy F, internal energy U, entropy S, and specific heat capacity C can be systematically computed with the help of the following relations:

$$F=-\frac{1}{\beta}\ln Z,\ U=-\frac{\partial\ln Z}{\partial\beta},\ S=\ln Z-\beta\frac{\partial\ln Z}{\partial\beta},\ C=\beta^2\frac{\partial^2\ln Z}{\partial\beta^2}. \tag{32}$$

Equation (32) can be reformulated in terms κ as follows:

$$\begin{aligned}\overline{F}(\kappa)&=\tfrac{F}{mc^2}=-\kappa\ln Z,\\ \overline{U}(\kappa)&=\tfrac{U}{mc^2}=\kappa^2\tfrac{\partial\ln Z}{\partial\kappa},\\ \overline{S}(\kappa)&=\tfrac{S}{K_B}=\ln Z+\kappa\tfrac{\partial\ln Z}{\partial\kappa},\\ \overline{C}(\kappa)&=\tfrac{C}{K_B}=2\kappa\tfrac{\partial\ln Z}{\partial\kappa}+\kappa^2\tfrac{\partial^2\ln Z}{\partial\kappa^2},\end{aligned} \tag{33}$$

It should be emphasized that for a very high temperature range $T\gg T_0$ (or $\beta\ll 1$), the deformation parameters's contribution remains negligible, and all terms in the sum of Eq. (28) have a positive power in β, which are very small compared with the term $\frac{2}{\mu m^2c^4\beta^2}\left(1+\beta mc^2\sqrt{\lambda}\right)$. Thus, one can approximate the partition function as

$$Z\simeq\frac{1}{2}+\frac{\sqrt{1-\frac{\mathscr{A}^2}{\mathscr{B}}\Theta l+\mathscr{B}\tau}}{\mathscr{A}}\kappa+\frac{\kappa^2}{\mathscr{A}}\simeq\frac{\kappa^2}{\mathscr{A}}=\frac{1}{\hbar\omega mc^2}\frac{1}{\beta^2}, \tag{34}$$

which leads to the following asymptotic limits of the mean energy U and the specific heat C:

$$U\simeq\frac{2}{\beta}=2K_BT,\ \text{and}\ C\simeq 2K_B. \tag{35}$$

For a very low temperature range, $T\ll T_0$ (or $\beta\gg 1$), we have

$$Z\simeq\left(\frac{1}{240}\frac{\mathscr{A}^3}{\left(1-\frac{\mathscr{A}^2}{\mathscr{B}}\Theta l+\mathscr{B}\tau\right)^{5/2}}-\frac{1}{12}\frac{\mathscr{A}}{\sqrt{1-\frac{\mathscr{A}^2}{\mathscr{B}}\Theta l+\mathscr{B}\tau}}\right)\frac{1}{\kappa}+\frac{1}{240}\frac{\mathscr{A}^3}{\left(1-\frac{\mathscr{A}^2}{\mathscr{B}}\Theta l+\mathscr{B}\tau\right)^{2}}\frac{1}{\kappa^2}$$
$$+\frac{1}{720}\frac{\mathscr{A}^3}{\left(1-\frac{\mathscr{A}^2}{\mathscr{B}}\Theta l+\mathscr{B}\tau\right)^{3/2}}\frac{1}{\kappa^3}, \tag{36}$$

and consequently the both U and C tend to zero, $U\to 0$, $C\to 0$.

Now, by introducing the following reducing parameters

$$\begin{cases}a=\frac{\sqrt{1-\frac{\mathscr{A}^2}{\mathscr{B}}\Theta l+\mathscr{B}\tau}}{\mathscr{A}},\ b=\frac{1}{\mathscr{A}},\ w=\frac{1}{1920}\frac{(2\mathscr{A})^3}{\left(1-\frac{\mathscr{A}^2}{\mathscr{B}}\Theta l+\mathscr{B}\tau\right)^{2}},\\ q=\frac{1}{720}\frac{\mathscr{A}^3}{\left(1-\frac{\mathscr{A}^2}{\mathscr{B}}\Theta l+\mathscr{B}\tau\right)^{3/2}},\ p=\frac{1}{240}\frac{\mathscr{A}^3}{\left(1-\frac{\mathscr{A}^2}{\mathscr{B}}\Theta l+\mathscr{B}\tau\right)^{5/2}}-\frac{1}{12}\frac{\mathscr{A}}{\sqrt{1-\frac{\mathscr{A}^2}{\mathscr{B}}\Theta l+\mathscr{B}\tau}},\end{cases} \tag{37}$$

the partition function (30) can be expressed as

$$Z(\kappa)=\frac{1}{2}+a\kappa+b\kappa^2+p\frac{1}{\kappa}+w\frac{1}{\kappa^2}+q\frac{1}{\kappa^3}. \tag{38}$$

Consequently, employing Eq. (38) in Eq. (33), the reduced thermal quantities become

$$\begin{aligned}
&\overline{F}(\kappa) = -\kappa \ln\left\{\tfrac{1}{2} + a\kappa + b\kappa^2 + \tfrac{p}{\kappa} + \tfrac{w}{\kappa^2} + \tfrac{q}{\kappa^3}\right\},\\
&\overline{U}(\kappa) = \tfrac{1}{Z}\left\{a\kappa^2 + 2b\kappa^3 - p - \tfrac{2w}{\kappa} - \tfrac{3q}{\kappa^2}\right\},\\
&\overline{S}(\kappa) = \ln\left\{\tfrac{1}{2} + a\kappa + b\kappa^2 + \tfrac{p}{\kappa} + \tfrac{w}{\kappa^2} + \tfrac{q}{\kappa^3}\right\} + \tfrac{1}{Z}\left\{a\kappa + 2b\kappa^2 - \tfrac{p}{\kappa} - \tfrac{2w}{\kappa^2} - \tfrac{3q}{\kappa^3}\right\},\\
&\overline{C}(\kappa) = \tfrac{2\kappa}{Z}\left\{a + 2b\kappa - \tfrac{p}{\kappa^2} - \tfrac{2w}{\kappa^3} - \tfrac{3q}{\kappa^4}\right\} + \tfrac{\kappa^2}{Z}\left\{2b + \tfrac{2p}{\kappa^3} + \tfrac{6w}{\kappa^4} + \tfrac{12q}{\kappa^5}\right\} - \tfrac{\kappa^2}{Z^2}\left\{a + 2b\kappa - \tfrac{p}{\kappa^2} - \tfrac{2w}{\kappa^3} - \tfrac{3q}{\kappa^4}\right\}^2.
\end{aligned} \tag{39}$$

It is evident that DNC and flat NC spaces influence the thermal quantities. Next, we thoroughly investigate the behavior of the obtained thermal quantities, presenting visual results and illustrating the various effects considered on these quantities.

It is also important to point out that when the KG oscillator system is subjected to a uniform magnetic field $\overrightarrow{B} = (0, 0, B)$, the momentum operator is modified via minimal coupling as $\overrightarrow{p} \to (\overrightarrow{p} - e\overrightarrow{A}/c)$. Here, the vector potential is taken in the symmetric gauge $\overrightarrow{A} = \frac{\overrightarrow{B}\times\overrightarrow{r}}{2} = \frac{B}{2}(-y, x, 0)$ with $\overrightarrow{r} = (x, y)$. Under this substitution, the KG oscillator system takes the following form:

$$\begin{aligned}
&\left\{\left(p_x + \tfrac{eB}{2c}y + im\omega x\right)\left(p_x + \tfrac{eB}{2c}y - im\omega x\right) + \left(p_y - \tfrac{eB}{2c}x + im\omega y\right)\left(p_y - \tfrac{eB}{2c}x - im\omega y\right)\right.\\
&\left. + (mc)^2 - \tfrac{E_{n,l}^2(B)}{c^2}\right\}\psi_{n,l}(\overrightarrow{r}) = 0.
\end{aligned} \tag{40}$$

Subsequently, by applying Eqs. (7) and (9), the system is brought into the DNC framework. With this setup, the magnetic behavior of the system can be systematically explored by analyzing the magnetization M, and magnetic susceptibility χ, which are defined as follows[52,53]:

$$M = \frac{1}{\beta}\frac{1}{Z}\frac{\partial \ln Z}{\partial \overrightarrow{B}}, \tag{41}$$

and

$$\chi = \frac{\partial M}{\partial \overrightarrow{B}}. \tag{42}$$

At absolute zero temperature $T = 0$, the magnetization reduces to[21,52]:

$$M = -\frac{\partial E_{n,l}^{\mathrm{DNC}}(B)}{\partial \overrightarrow{B}}, \tag{43}$$

where $E_{n,l}^{\mathrm{DNC}}(B)$ represents the energy of the system within the DNC framework under the presence of B. It is worth noting that magnetization is often used to examine the possibility of phase transitions, while magnetic susceptibility quantifies how much a material becomes magnetized under an applied magnetic field. Susceptibility also helps clarify the nature of a phase transition, if it exists.

Graphical analysis and discussion

Based on the obtained numerical results, we present plots illustrating the thermal behavior and partition function of the deformed KG oscillator under varying thermal (β), quantum (ω), and deformation (Θ, τ) parameters. The constants are set as $\hbar = c = 1$ (natural units), and $\mathscr{B} = l = 1$. Accordingly, $\mathscr{A} = \omega/m$, serves as a parameter controlling the non-relativistic limit and, for simplicity, is used in place of ω to represent quantum-relativistic effects. As reported in[54–56], the values of $\mathscr{A}$ determine whether the system is in the relativistic region or in the non-relativistic one. In our work, as in[56] and others, one can distinguish two regions : the first, defined by $\mathscr{A} \geq 0.5$, corresponds to the relativistic regime, and the other, with $\mathscr{A} < 0.5$, represents the non-relativistic regime. Note that in commutative case, Boumali[56] studied the thermal properties of the relativistic harmonic oscillator including KG oscillator in one dimension. He derived the thermodynamics quantities by using the Euler-MacLaurin approximation, and the formalism employed covered the entire range of temperatures through the use of the Hurwitz zeta function method. Note that adopting κ instead of T in our calculations simplifies the plots and allows the use of dimensionless thermal quantities. Additionally, employing natural units enables for reduced dimensionless DNC and NC parameters, defined as $\tau \equiv \tau l_p^2$ and $\Theta \equiv \Theta/l_p^2$, where l_p denotes Planck length.

The partition function (Eq. (30)) is illustrated in Figs. 1–3. The reduced thermal quantities (Eq. (39)) are depicted in Figs. 4–15. Note that in all the plots involving $\mathscr{A}$, red and black dashed lines represent the non-relativistic regime, while solid lines of other colors are used for the relativistic regime.

In Fig. 1, the partition function Z is plotted separately as a function of κ and $\mathscr{A}$, with Θ and τ held fixed. In Fig. 2, Z is plotted versus κ for a fixed $\mathscr{A}$, and the results are shown for different values of Θ and τ. Fig. 3 extend this analysis, showing the dependence of Z on Θ and τ across varying $\mathscr{A}$ and κ.

From sub-fig (1.a) Z increases monotonically with κ for all values of $\mathscr{A}$, as expected. For the non-relativistic regime, the growth of Z is much more rapid with increasing κ. As $\mathscr{A}$ increases, the curves flatten and the magnitude of Z is reduced, and the thermal response of the system becomes more stable or less sensitive to changes in κ. In sub-fig (1.b), the most striking feature is the sharp peak at $\mathscr{A} = 3.3$ for all values of κ, shown in the zoomed inset. This confirms a critical point where Z sharply increases, possibly due to a resonance or singularity in the denominator. This reveals that small κ values lead to very large Z near the critical point, suggesting a diverging thermodynamic response that could be linked to a phase transition–like behavior. The

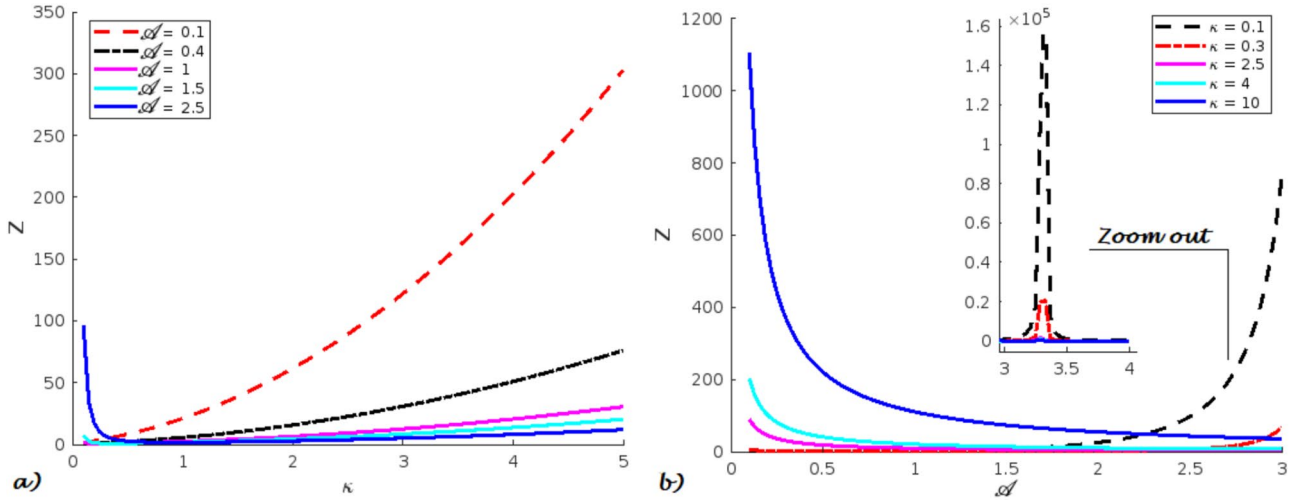

Fig. 1. The partition function Z as a function of κ & $\mathscr{A}$ separately, with fixed values of $\Theta = \tau = 0.1$. (**a**) Variation of Z with respect to κ for different values of $\mathscr{A}$; (**b**) variation of Z with respect to $\mathscr{A}$ for different values of κ.

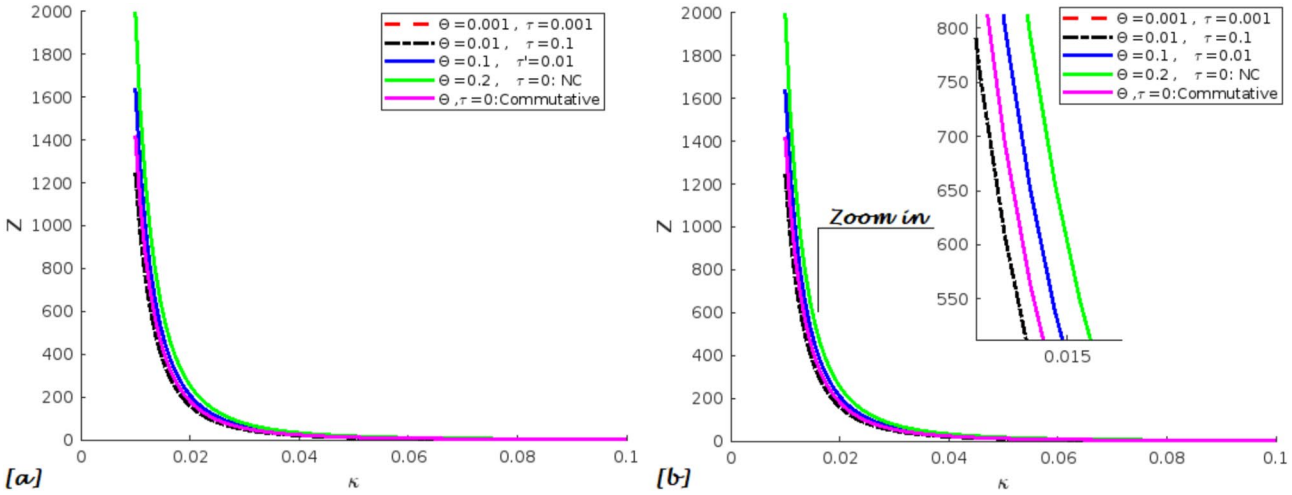

Fig. 2. The partition function Z as a function of κ, shown for different values of NC & DNC parameters Θ & τ. (**a**) Non-relativistic case, $\mathscr{A} = 0.1$; (**b**) relativistic case, $\mathscr{A} = 1.5$.

presence of a peak at $\mathscr{A} = 3.5$ regardless of κ implies that this value corresponds to a universal feature of the system, likely tied to the structure of the DNC space. The suppression of Z at high $\mathscr{A}$ (relativistic regime) and the enhancement at low $\mathscr{A}$ (non-relativistic regime), especially for small κ, show how strongly the thermodynamic state density is modulated by both parameters. From Fig. 2, Z shows a similar increasing trend with κ in both the non-relativistic and relativistic regimes. The effect of the DNC and NC parameters appears consistent across both cases, indicating that the deformation effects on Z are comparable regardless of the relativistic scale. In Fig. 3, as κ increases, the overall magnitude and surface curvature of Z change significantly, indicating a strong interplay between the DNC/NC parameters and the oscillator strength. More precisely, Z exhibits noticeable variations with respect to the DNC and NC parameters, depending on the value of κ. Increasing κ alters both the amplitude and shape of the surface, highlighting the sensitivity of the system's thermodynamic behavior to deformation effects.

We plot the free energy $\overline{F}$, internal energy $\overline{U}$, entropy $\overline{S}$, and specific heat capacity $\overline{C}$ as functions of the parameters κ and $\mathscr{A}$ separately, with Θ and τ held fixed in Figs. 4, 7, 10, and 13 respectively.

In Figs. 5, 8, 11, and 14, the same quantities— $\overline{F}$, $\overline{U}$, $\overline{S}$, and $\overline{C}$ respectively—are plotted versus κ for a fixed $\mathscr{A}$, showing the effects each Θ and τ.

Finally, Figs. 6, 9, 12, and 15 extend the analysis by illustrating the dependence of $\overline{F}$, $\overline{U}$, $\overline{S}$, and $\overline{C}$, respectively on Θ and τ, across varying $\mathscr{A}$ and κ.

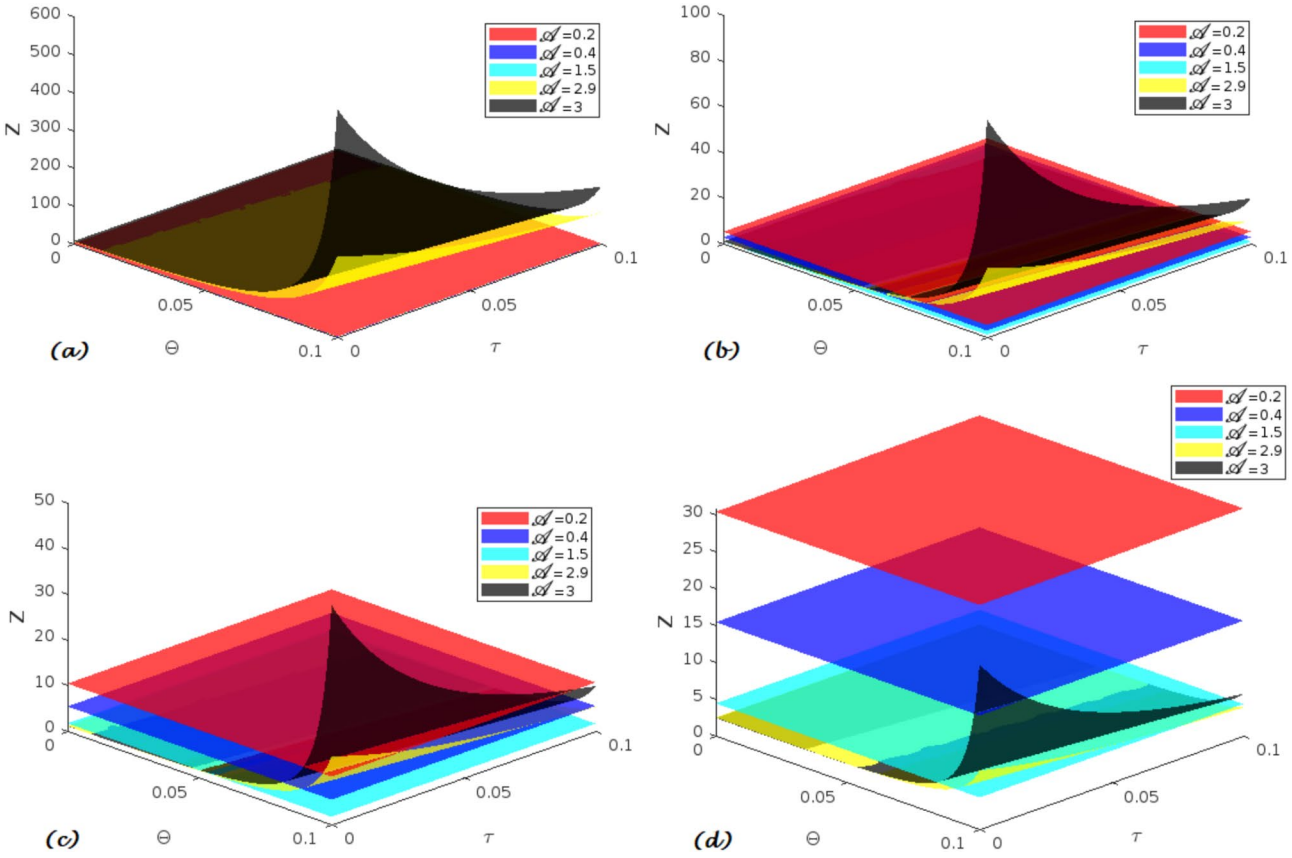

Fig. 3. 3D plot of the partition function Z as a function of NC & DNC parameters Θ & τ, shown for different values of $\mathscr{A}$. (**a**) $\kappa = 0.2$; (**b**) $\kappa = 0.6$; (**c**) $\kappa = 1$; (d) $\kappa = 2$.

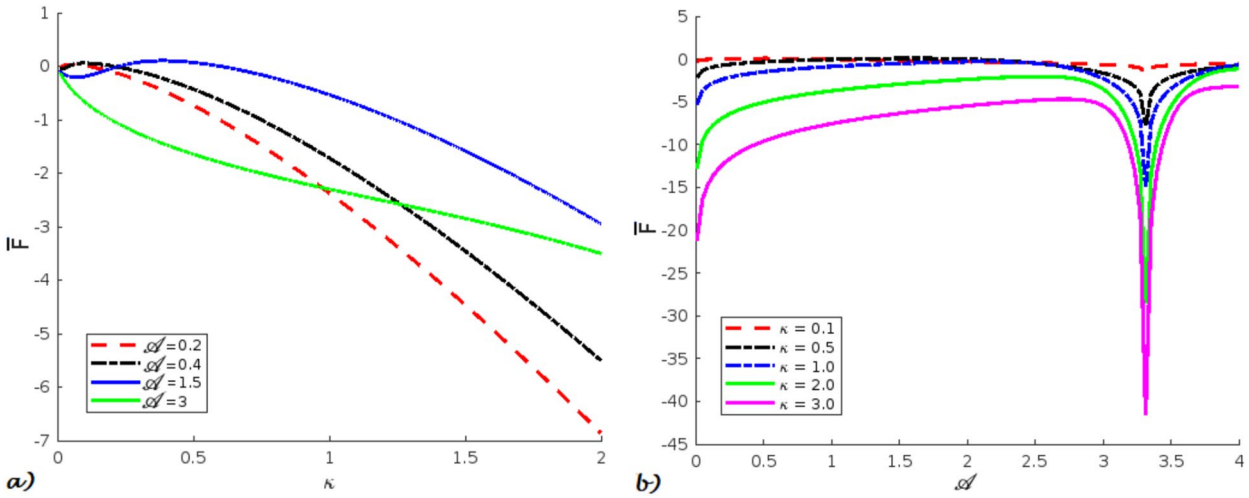

Fig. 4. The free energy $\overline{F}$ as a function of κ and $\mathscr{A}$ separately, with fixed values of $\Theta = \tau = 0.1$. (**a**) Variation of $\overline{F}$ with respect to κ for different values of $\mathscr{A}$; (**b**) variation of $\overline{F}$ with respect to $\mathscr{A}$ for different values of κ.

It is noteworthy to highlight that in our calculations and plots, the expression $1 - \frac{\mathscr{A}^2}{\mathscr{B}}\Theta l + \mathscr{B}\tau$, which appears under square roots and raised to fractional powers in the thermal quantities, remains positive and real for the typical values of $\mathscr{A}$, Θ, and τ used in this work.

The plots in Fig. 4 show that the free energy $\overline{F}$ exhibits non-monotonic behavior with respect to both κ and $\mathscr{A}$, featuring a clear minimum (or dip) at intermediate values. This indicates the existence of an optimal point where the system's thermodynamic stability is enhanced, as $\overline{F}$ increases again for larger values of either

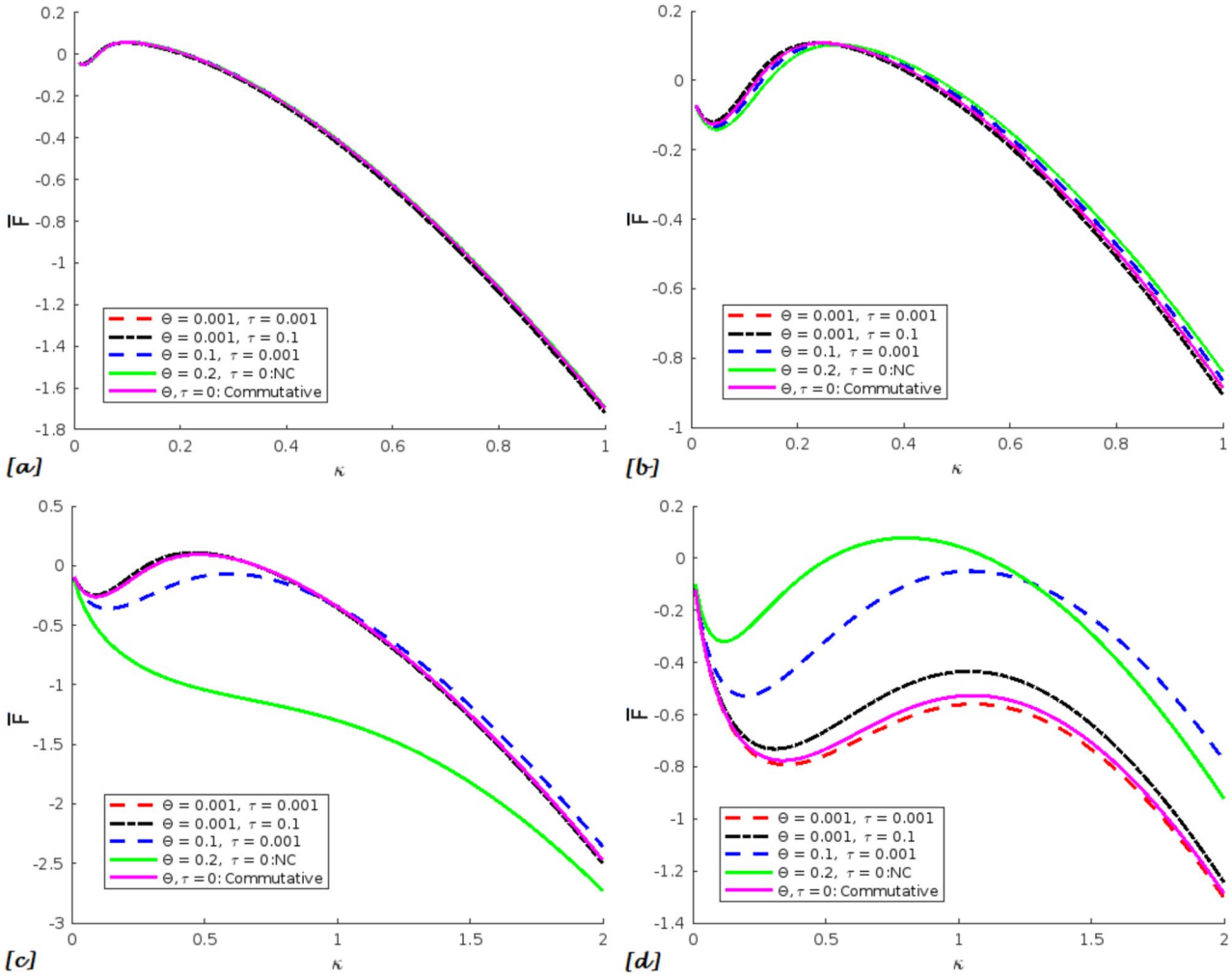

Fig. 5. The free energy $\overline{F}$ as a function of κ, shown for different values of Θ & τ. (**a**): Non-relativistic case, $\mathscr{A} = 0.1$; (**b**), (**c**), and (**d**): relativistic cases with $\mathscr{A} = 1, 2, 5$, respectively.

parameter. In contrast, the plots in Fig. 5 show that $\overline{F}$ decreases monotonically with increasing κ across all cases. The magnitude of $\overline{F}$ is more pronounced in the relativistic regime ($\mathscr{A} = 1, 2, 5$), particularly for higher deformation parameters Θ and τ. Sensitivity to these deformation parameters becomes more significant as $\mathscr{A}$ increases. Overall, $\overline{F}$ exhibits consistent qualitative behavior while becoming steeper with increasing relativistic effects. The 3D plots in Fig. 6 reveal that $\overline{F}$ generally decreases as both Θ and τ increase, indicating that deformation effects reduce the system's energy. This trend becomes more pronounced at higher values of κ, especially in plot (6.d). Additionally, the curvature of the surfaces intensifies with increasing $\mathscr{A}$, suggesting stronger thermodynamic sensitivity in relativistic regimes. In summary, $\overline{F}$ demonstrates a smooth, nonlinear dependence on both the NC and DNC parameters.

Figure 7 shows that the internal energy $\overline{U}$ monotonically increases with increasing κ and decreases with $\mathscr{A}$. However, in subplot (7.b), a slight non-monotonic behavior appears in the range $\mathscr{A} \in [3, 3.7]$, clearly more pronounced for $\kappa = 1.5$ and 3, where $\overline{U}$ exhibits a shallow dip before continuing to decrease—hinting at a transitional effect in the system's thermodynamics for intermediate relativistic strengths. Fig. 8 demonstrates that $\overline{U}$ increases with the deformation parameters Θ and τ, especially in the relativistic regimes ($\mathscr{A} = 2, 5, 15$). The effect is minimal in the non-relativistic case (8.a), but becomes more pronounced as $\mathscr{A}$ increases, highlighting enhanced sensitivity to deformation in relativistic settings. In Fig. 9, the 3D plots show that $\overline{U}$ decreases as both Θ and τ increase, with this trend becoming more pronounced at higher values of κ. The energy surfaces become steeper as κ grows, indicating stronger sensitivity to deformation parameters in highly NC regimes.

Subplot (10.a) interestingly reveals a contrasting behavior of the entropy $\overline{S}$: in the non-relativistic regime, S increases with κ, whereas in the relativistic regime it decreases. Precisely, the curves for $\mathscr{A} = 1.5$ and 3 deviate from this trend, displaying non-monotonic behavior. In subplot (10.b), $\overline{S}$ decreases as a function of $\mathscr{A}$, but a noticeable peak appears around $\mathscr{A} = 3.3$, indicating a nontrivial interplay between relativistic and thermal contributions near this regime. The plots in Fig. 11 show that the effect of the deformation parameters Θ and τ on $\overline{S}$ is minimal in the non-relativistic regime but becomes significant as $\mathscr{A}$ increases. Similarly, Fig. 12 demonstrates that the influence of both Θ and τ on $\overline{S}$ is negligible in the non-relativistic regime, while it

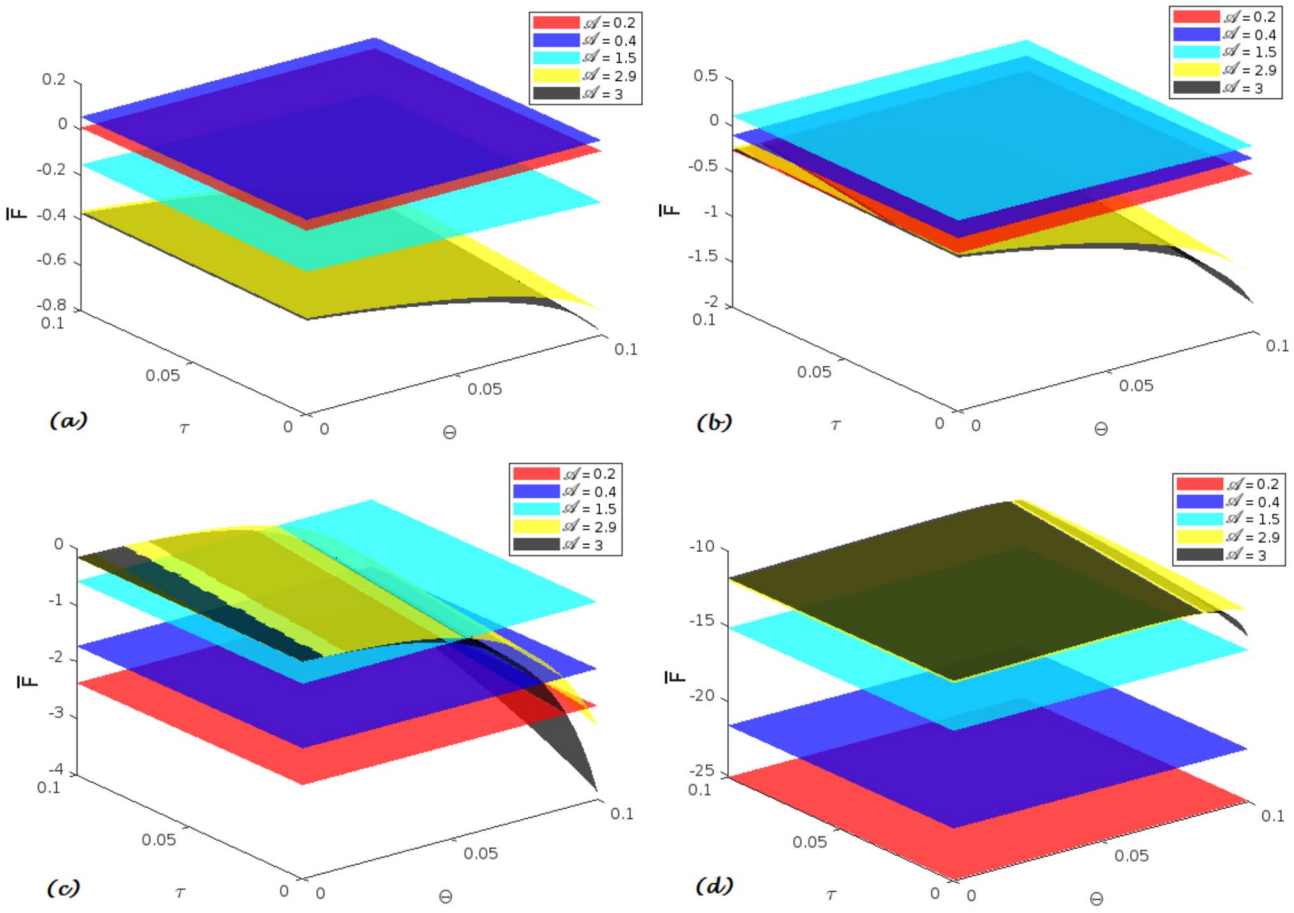

Fig. 6. 3D plot of the free energy $\overline{F}$ as a function of Θ & τ, shown for different values of $\mathscr{A}$. (**a**) $\kappa = 0.1$; (**b**) $\kappa = 0.3$; (**c**) $\kappa = 1$; (**d**) $\kappa = 5$.

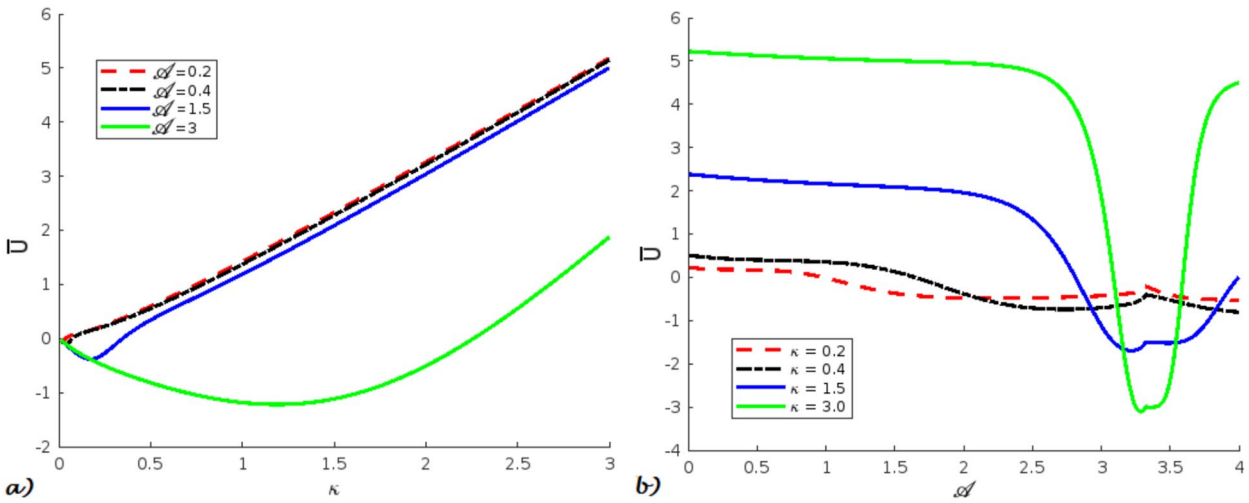

Fig. 7. The internal energy $\overline{U}$ as a function of κ and $\mathscr{A}$ separately, with fixed values of $\Theta = \tau = 0.1$. (**a**) Variation of $\overline{U}$ with respect to κ for different values of $\mathscr{A}$; (**b**) the variation is with respect to $\mathscr{A}$ for different values of κ.

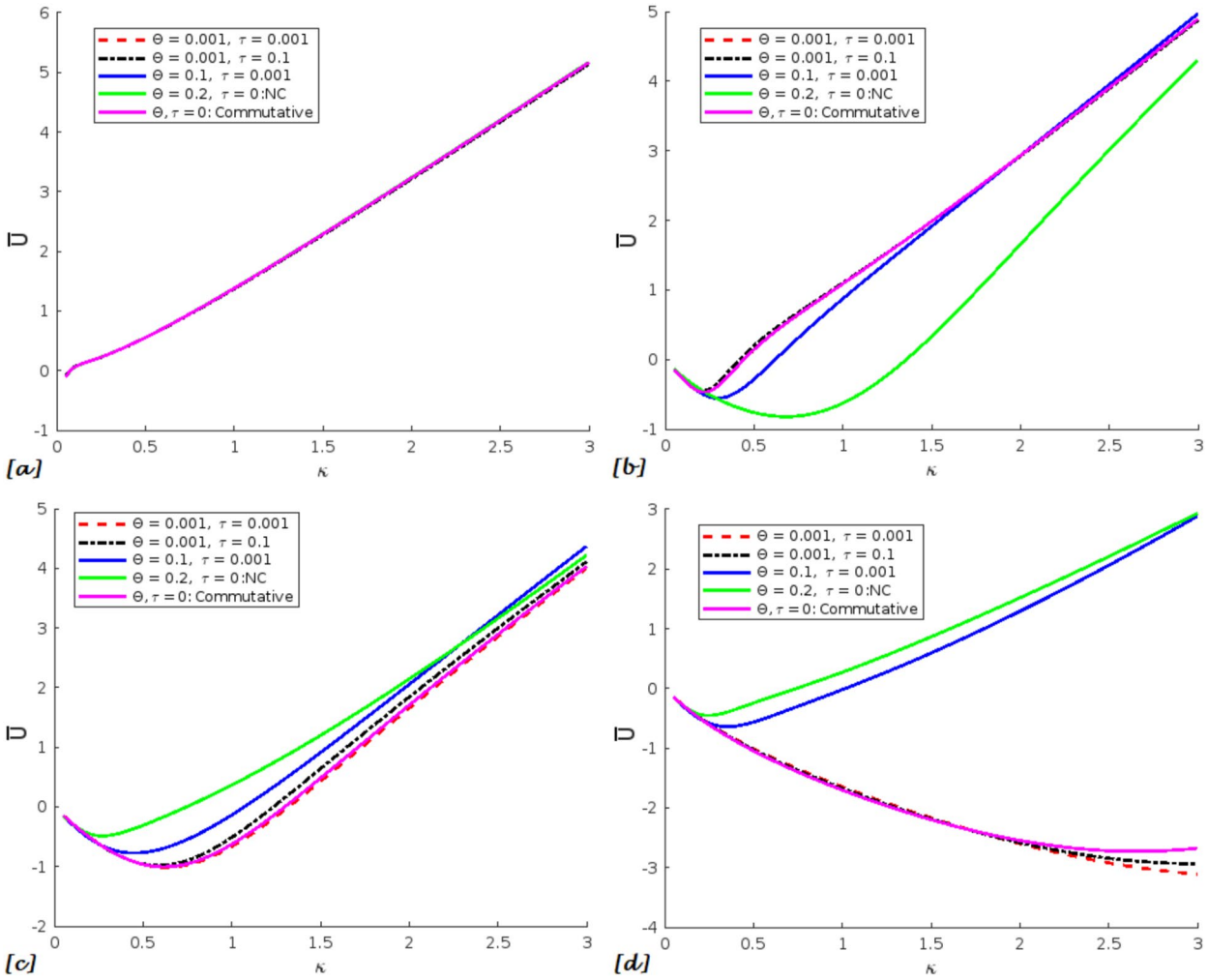

Fig. 8. The internal energy $\overline{U}$ as a function of κ, shown for different values of Θ & τ. (**a**): Non-relativistic case, $\mathscr{A} = 0.1$; (**b**), (**c**), and (**d**): relativistic cases with $\mathscr{A} = 2, 5, 15$, respectively.

becomes considerable in the relativistic regime, especially as these parameters increase. This trend becomes more pronounced with increasing κ.

Subplot (13.a) shows a non-monotonic behavior of the specific heat capacity $\overline{C}$ with respect to κ, featuring a slight initial increase followed by a rapid decrease. It is evident that the relativistic regime has a more pronounced effect on the trend compared to the non-relativistic case. In subplot (13.b), $\overline{C}$ also exhibits non-monotonic behavior as a function of $\mathscr{A}$, with a noticeable dip near zero appearing around $\mathscr{A} = 3.3$. Interestingly, all the curves converge toward this point before increasing again, and this behavior becomes more prominent as the thermal parameter κ increase. The plots in Fig. 14 show that the effect of the deformation parameters Θ and τ on $\overline{C}$ is minimal in the non-relativistic regime but becomes significant in the relativistic cases as $\mathscr{A}$ increases. Similarly, Fig. 15 also demonstrates that the influence of Θ and τ on $\overline{C}$ is negligible in the non-relativistic regime but becomes substantial in the relativistic regime, particularly for $\mathscr{A} = 2.9$ or 3. This trend is further intensified as κ increases.

When analyzing the data, it appears that the behavior of the thermal quantities exhibits significant variations and rich structural features. The results clearly demonstrate how thermal, quantum, or deformation-induced fluctuations dominate in different regimes—both non-relativistic and relativistic. The plots consistently reveal distinct patterns under the influence of DNC and flat NC deformations.

Moreover, when comparing our more general results with those in[54], which explores the thermal properties of the KG system within a commutative framework, we observe excellent agreement in the corresponding plots. In particular, our results in the commutative case ($\Theta = \tau = 0$, shown as magenta lines) match those of[54]. For instance, our plots for $\overline{F}$ (Fig.5), $\overline{U}$ (Fig.8), and $\overline{S}$ (Fig.11) align closely with $\overline{F}$ (Fig.2), $\overline{U}$ (Fig.3) and $\overline{S}$ (Fig.4) in[54], respectively. Similar consistency is found across the remaining plots. This agreement strongly supports the validity of our thermal analysis and visualization.

It is important to emphasize that the vanishing of the internal energy U and specific heat capacity C at low temperatures (or equivalently, low κ) reflects the suppression of thermal excitation in both the DNC and flat NC frameworks. This behavior is consistent with the third law of thermodynamics, which states that as T approaches

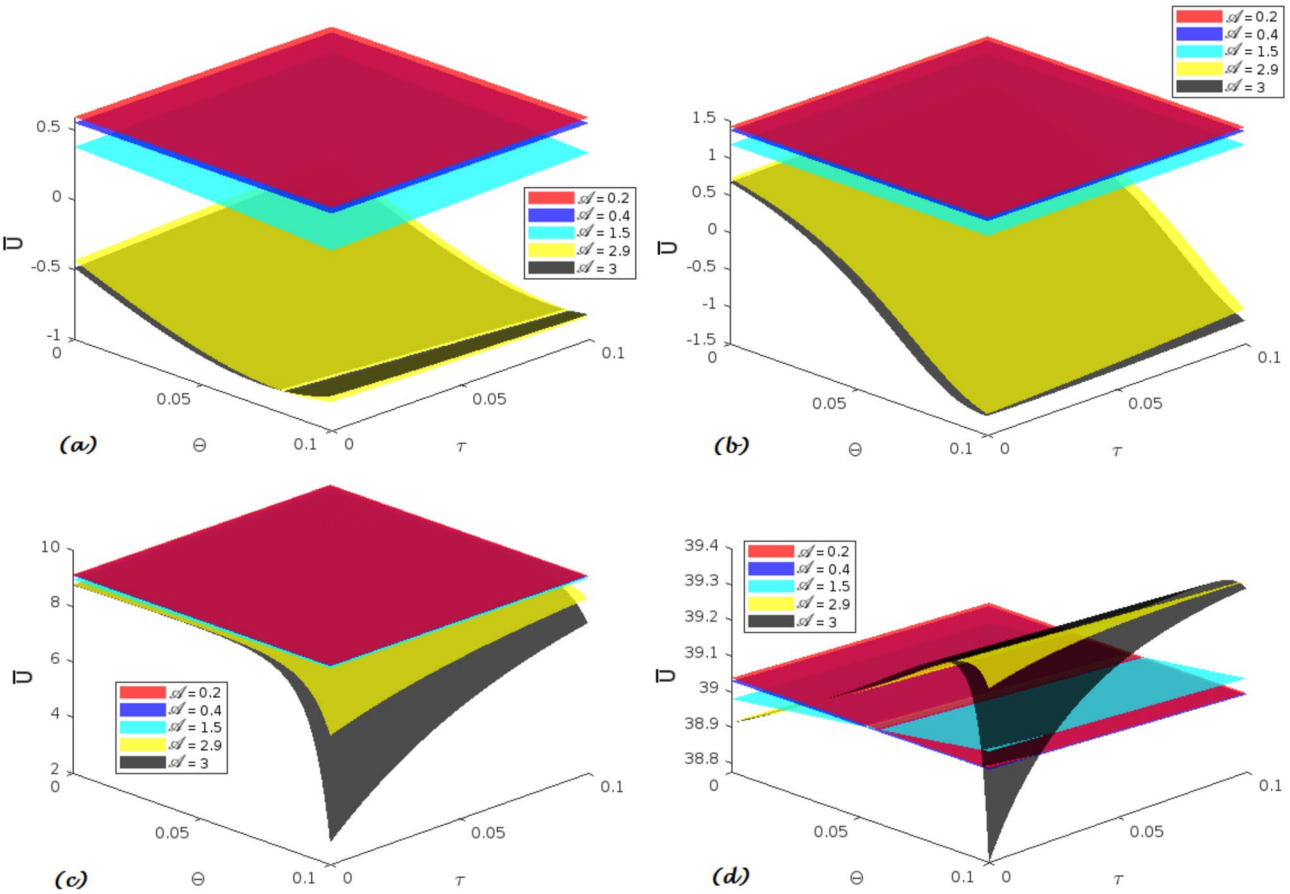

Fig. 9. 3D plot of the internal energy $\overline{U}$ as a function of Θ & τ, shown for different values of $\mathscr{A}$. (**a**) $\kappa = 0.5$; (**b**) $\kappa = 1$; (**c**) $\kappa = 5$; (**d**) $\kappa = 20$.

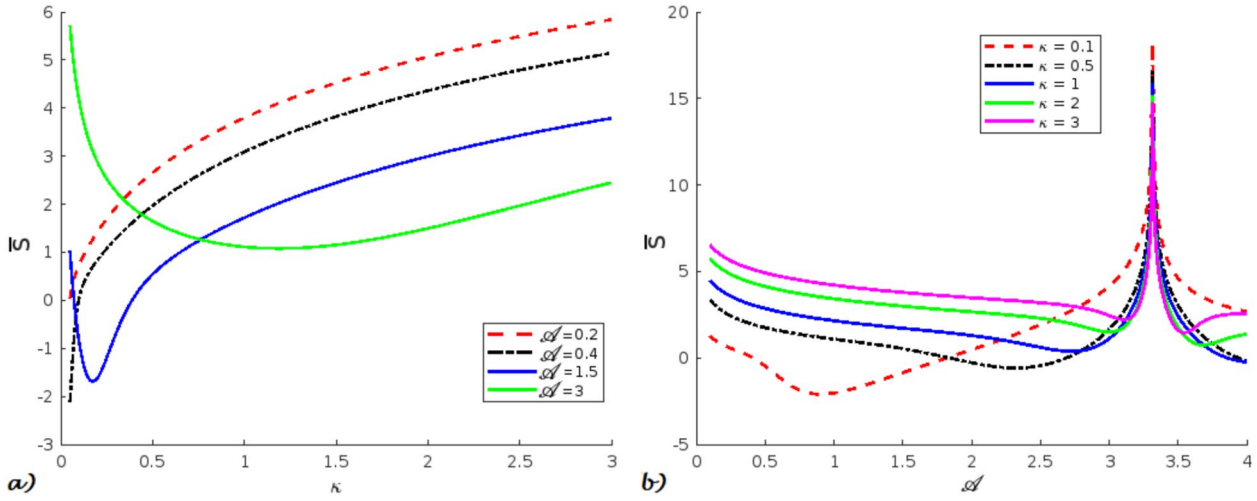

Fig. 10. The entropy $\overline{S}$ as a function of κ and $\mathscr{A}$ separately, with fixed values of $\Theta = \tau = 0.1$. (**a**) Variation of $\overline{S}$ with respect to κ for different values of $\mathscr{A}$; (**b**) the variation of $\overline{S}$ is with respect to $\mathscr{A}$ for different values of κ.

absolute zero, entropy, and therefore thermal fluctuations, tends to vanish. In this regime, only the lowest energy levels i.e., the ground state, are populated, leaving no energy available for thermal distribution, and thus $U \to 0$ and $C \to 0$. From a deeper perspective, this thermodynamic suppression is influenced by the deformation parameters Θ and τ, which modify the energy spectrum and density of states (see Eqs. (18) & (19)). Nevertheless,

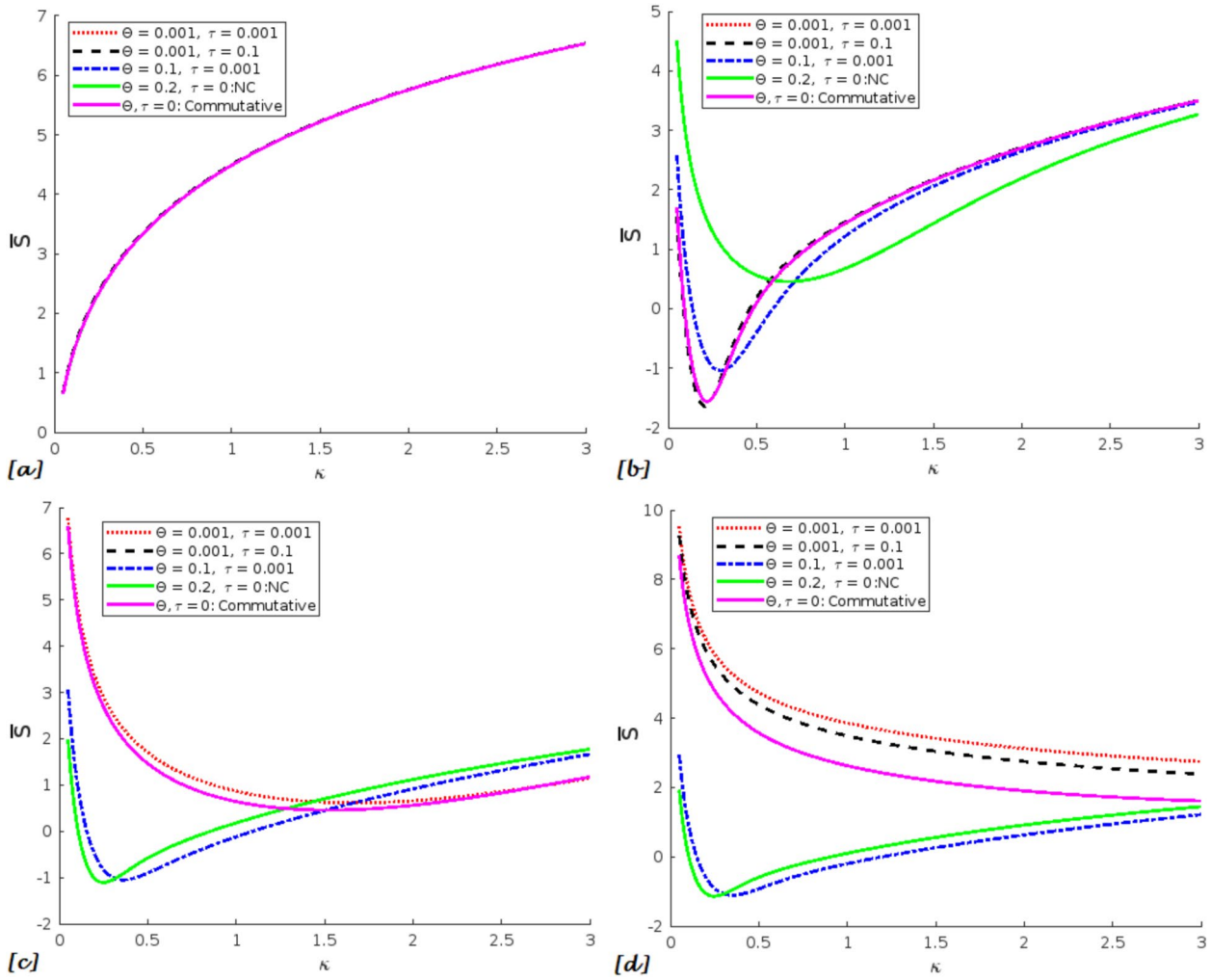

Fig. 11. The entropy $\overline{S}$ as a function of κ, shown for different values of Θ & τ. (**a**): Non-relativistic case, $\mathscr{A} = 0.1$; (**b**), (**c**), and (**d**): relativistic cases with $\mathscr{A} = 2, 10, 20$, respectively.

our numerical results indicate that even when the deformation parameters are fixed e.g., $\Theta = \tau = 0.1$, the suppression of thermal activity at low temperatures persists across a wide range of $\mathscr{A}$ values. This indicates that the vanishing of U and C in the low-temperature regime is a robust and generic feature of the deformed KG oscillator model. Similar trends have also been observed in other quantum systems under deformation, including the KG oscillator in NC space[22] and cosmological string-inspired backgrounds[21]. Physically, DNC deformation typically shifts or reshapes the energy spectrum but do not eliminate the energy gap between the ground and excited states. As long as the spectrum remains discrete (quantized) and bounded from below (i.e., with a well-defined ground state and no energy states exist below it), the suppression of thermal activity at low temperatures remains a universal characteristic. This feature is essential for ensuring thermodynamic stability.

Finally, the plots vividly highlight the intricate interplay between quantum-relativistic, thermal, and deformation effects throughout the thermal system's behavior.

Conclusion

In this work, we have numerically investigated the 2D thermal behavior of the KG oscillator system within the framework of DNC space. First, we reviewed and utilized the energy spectrum energy of the deformed KG oscillator determined in our previous study[14]. Using this spectrum, we evaluated the numerical partition function and, subsequently, derived the thermal properties, including the free energy, internal energy, entropy, and specific heat capacity. The effects of DNC and flat NC spaces on these properties were thoroughly analyzed and discussed. The visual representations reveal a rich and nontrivial behavior of the system in DNC and flat NC spaces, characterized by mixed fluctuations arising from thermal, quantum-relativistic, and deformation effects. They suggest zones of stability and instability, as well as patterns of monotonicity and non-monotonicity, which are significant for both theoretical insights and potential physical applications. Additionally, the vanishing behavior of internal energy and specific heat at low temperatures supports the thermodynamic consistency of the modified energy spectrum. This suggests that the DNC and flat NC corrections do not lead to unphysical behavior in the low-energy limit, further reinforcing the idea that both DNC and flat NC deformations respect

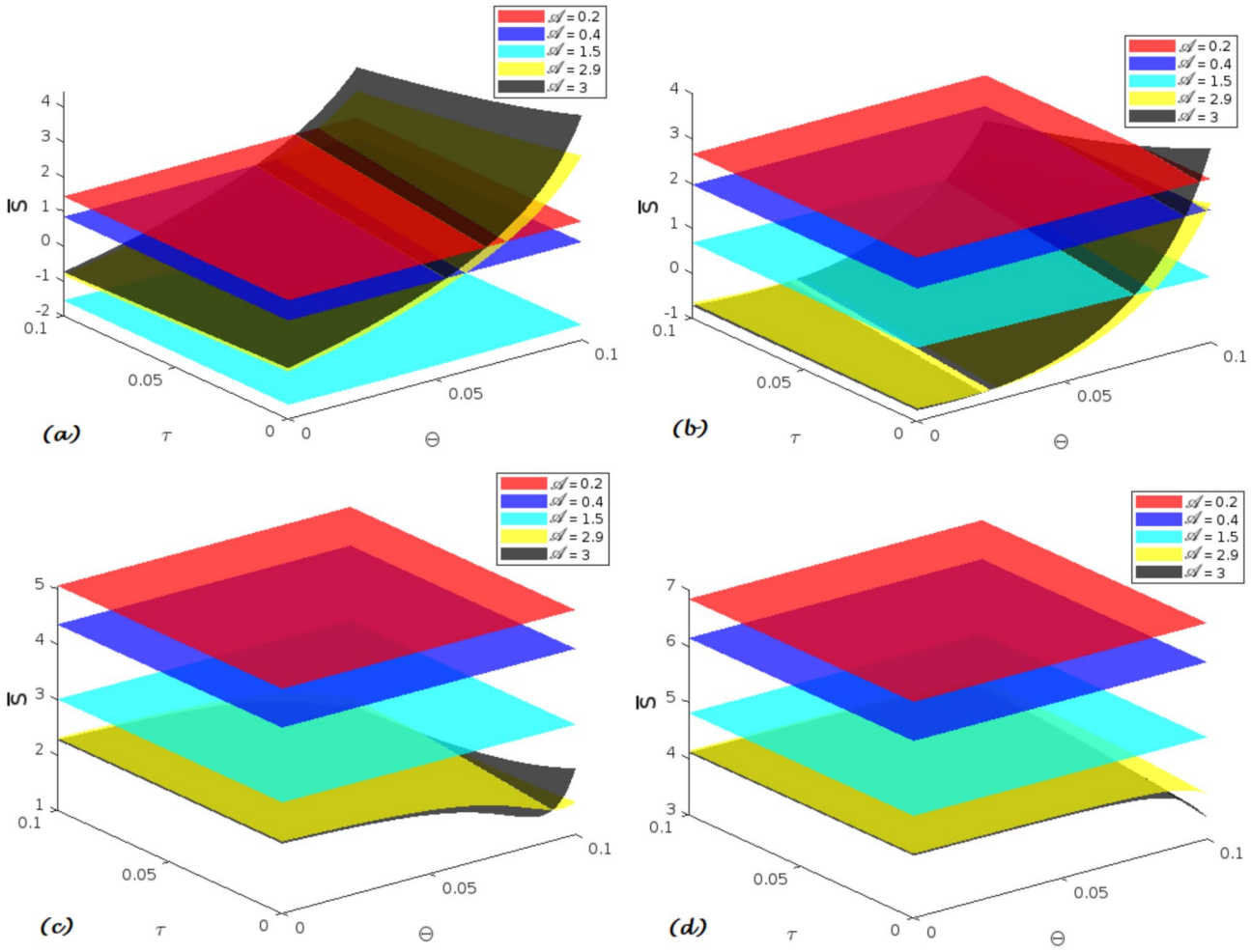

Fig. 12. 3D plot of the entropy $\overline{S}$ as a function of Θ & τ, shown for different values of $\mathscr{A}$. (**a**) $\kappa = 0.2$; (**b**) $\kappa = 0.5$; (**c**) $\kappa = 2$; (**d**) $\kappa = 5$.

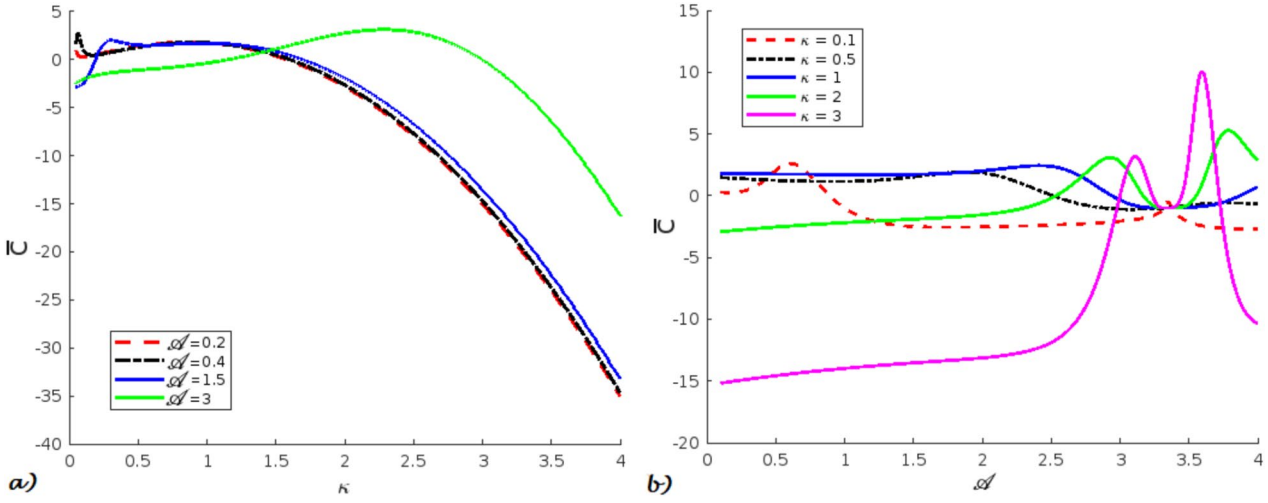

Fig. 13. The specific heat capacity $\overline{C}$ as a function of κ and $\mathscr{A}$ separately, with fixed values of $\Theta = \tau = 0.1$. (**a**) Variation of $\overline{C}$ with respect to κ for different values of $\mathscr{A}$; (**b**) the variation of $\overline{C}$ is with respect to $\mathscr{A}$ for different values of κ.

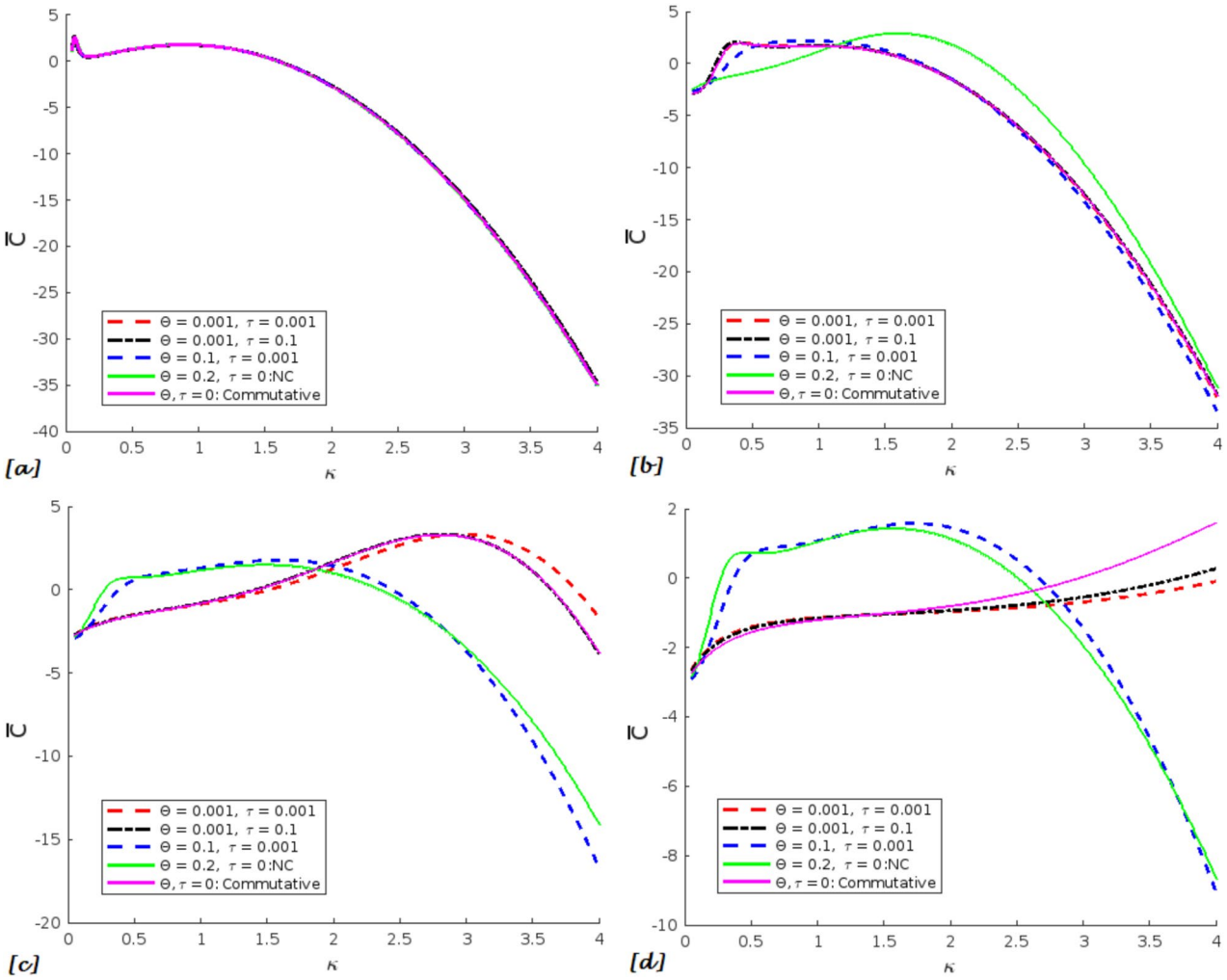

Fig. 14. The specific heat capacity $\overline{C}$ as a function of κ, shown for different values of Θ & τ. (**a**): Non-relativistic case, $\mathscr{A} = 0.4$; (**b**), (**c**), and (**d**): relativistic cases with $\mathscr{A} = 2, 10, 20$, respectively.

fundamental thermodynamic constraints. Notably, investigating fundamental phenomena in DNC space is of particular interest, as objects in such a setting naturally exhibit string-like behavior—one of the key motivations for studying DNC geometry. Our findings can be used to explore the thermodynamical properties of other systems within DNC space. Furthermore, as discussed in Sect. 2, certain operators in the DNC framework are non-Hermitian. The interplay between DNC framework, non-Hermiticity theory, thermodynamic properties, and string theory may open up promising directions for future research.

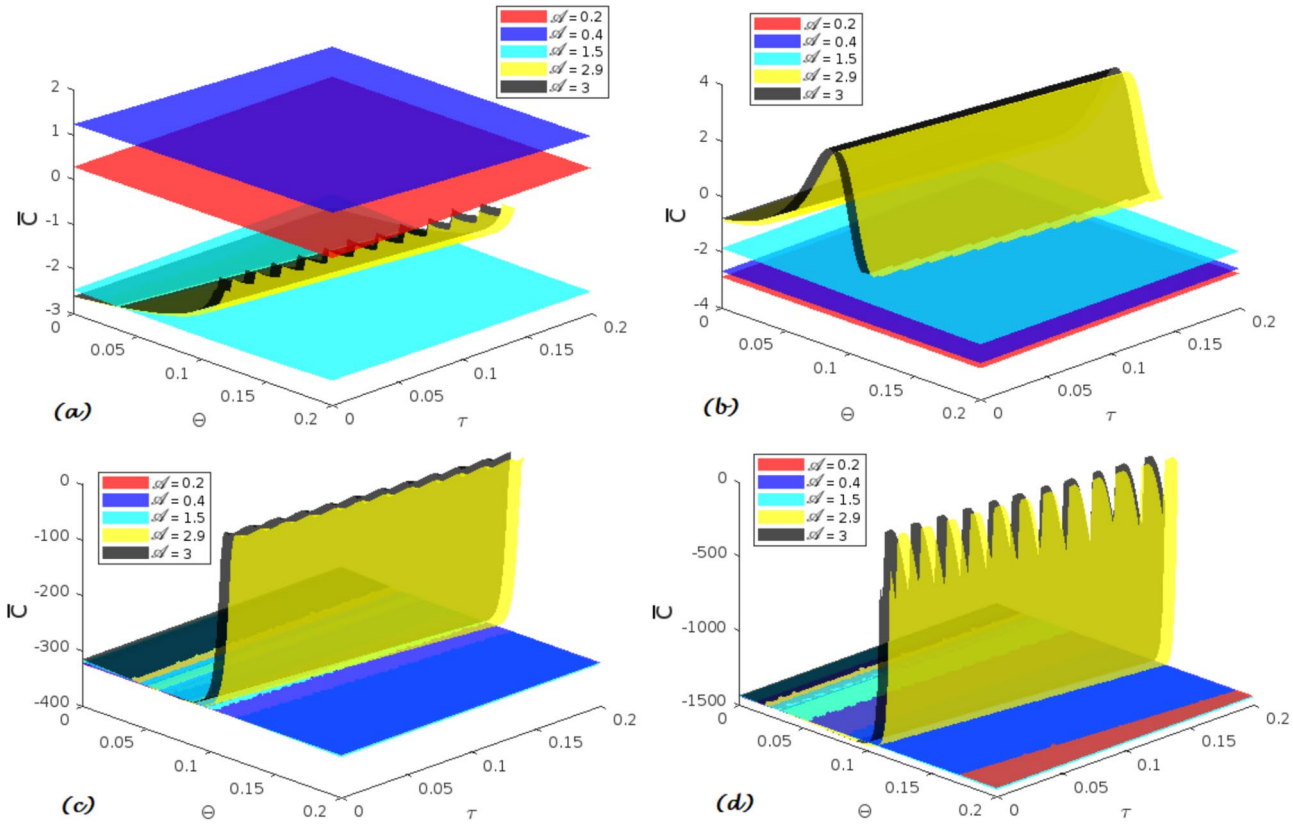

Fig. 15. 3D plot of the specific heat capacity $\overline{C}$ as a function of Θ & τ, shown for different values of $\mathscr{A}$. (**a**) $\kappa = 0.1$; (**b**) $\kappa = 2$; (**c**) $\kappa = 10$; (**d**) $\kappa = 20$.

Data availability

The datasets used and analysed during the current study are available from the corresponding author on reasonable request.

Received: 28 April 2025; Accepted: 2 July 2025
Published online: 06 August 2025

References

1. Bruce, S. & Minning, P. *The Klein-Gordon oscillator. Nuov. Cim. A* **106**, 711. https://doi.org/10.1007/BF02787240 (1993).
2. Dvoeglazov, V. V. Comment on the Klein-Gordon oscillator by S. Bruce and P. Minning. *Il Nuovo Cimento A***107**, 1411. https://doi.org/10.1007/BF02775780 (1994).
3. Mirza, B. & Mohadesi, M. The Klein-Gordon and the Dirac oscillators in a noncommutative space. *Commun. Theor. Phys.***42**(5), 664. https://doi.org/10.1088/0253-6102/42/5/664 (2004).
4. Chargui, Y. et al. Exact solution of D-dimensional Klein-Gordon oscillator with minimal length. *Commun. Theor. Phys.***53**(2), 231. https://doi.org/10.1088/0253-6102/53/2/05 (2010).
5. Cheng, J. Y. $\mathcal{PT}$-Symmetric Klein-Gordon oscillator. *Int. J. Theor. Phys* **50**, 228. https://doi.org/10.1007/s10773-010-0512-1 (2011).
6. Liang, M. L. & Yang, R. L. Three-dimensional Klein-Gordon oscillator in a background magnetic field in noncommutative phase space. *Int. J. Mod. Phys. A***27**, 1250047. https://doi.org/10.1142/S0217751X12500479 (2012).
7. Bakke, K. & Furtado, C. On the Klein-Gordon oscillator subject to a Coulomb-type potential. *Ann. Phys.***355**, 48. https://doi.org/10.1016/j.aop.2015.01.028 (2015).
8. Carvalho, J. et al. Klein-Gordon oscillator in Kaluza-Klein theory. *Eur. Phys. J. C Part. Fields***76**365. https://doi.org/10.1140/epjc/s10052-016-4189-3 (2016).
9. Wang, B. Q. et al. Klein-Gordon oscillator with position-dependent mass in the rotating cosmic string spacetime. *Mod. Phys. Lett. A***33**, 1850025. https://doi.org/10.1142/S0217732318500256 (2018).
10. Santos, L. C. N. et al. Klein-Gordon oscillator in a topologically nontrivial space-time. *Adv. High Energy Phys.*https://doi.org/10.1155/2019/2729352 (2019).
11. Leite, E. V. B. et al. Klein-Gordon oscillator under the effects of the Cornell-type interaction in the Kaluza-Klein theory. *Braz. J. Phys.***50**, 744. https://doi.org/10.1007/s13538-020-00785-4 (2020).
12. Mota, R. D. et al. Landau levels for the (2+1) Dunkl-Klein-Gordon oscillator. *Mod. Phys. Lett. A***36**, 2150066. https://doi.org/10.1142/S0217732321500668 (2021).
13. de Montigny, M. et al. Klein-Gordon oscillator in a global monopole space-time with rainbow gravity. *Eur. Phys. J. Plus* **137**, 54. https://doi.org/10.1140/epjp/s13360-021-02251-9 (2022).
14. Haouam, I. Klein-Gordon oscillator in dynamical noncommutative space. *Int. J. Theor. Phys.***63**174. https://doi.org/10.1007/s10773-024-05696-7 (2024).

15. Ahmed, F. & Bouzenada, A. Quantum dynamics of spin-0 particles in a cosmological space-time. *Nucl. Phys. B.***1000**, 116490. https://doi.org/10.1016/j.nuclphysb.2024.116490 (2024).
16. Ahmed, F. & Bouzenada, A. Study of scalar particles through the Klein-Gordon equation under rainbow gravity effects in Bonnor-Melvin-Lambda space-time. *Commun. Theor. Phys.***76**(4), 045401. https://doi.org/10.1088/1572-9494/ad2e88 (2024).
17. Ahmed, F. & Bouzenada, A. Scalar fields in Bonnor-Melvin-Lambda universe with potential: A study of dynamics of spin-zero particles-antiparticles. *Phys. Scr.***99**(6), 065033. https://doi.org/10.1088/1402-4896/ad4830 (2024).
18. Ahmed, F. & Bouzenada, A. PDM relativistic quantum oscillator in Einstein-Maxwell-Lambda space-time. *Int. J. Geom. Methods Mod. Phys.* **22**(01), 2450253. https://doi.org/10.1142/S0219887824502530 (2025).
19. Hemame, Z. et al. Exact solutions of D-dimensional Klein-Gordon oscillator with Snyder-de Sitter algebra. *J. Math. Phys.***61**, 102301. https://doi.org/10.1063/5.0015150 (2020).
20. Zaim, S. et al. Negative heat capacity for a Klein-Gordon oscillator in non-commutative complex phase space. *Int. J. Geom. Methods Mod. Phys.***14**, 1750141. https://doi.org/10.1142/S0219887817501419 (2017).
21. Bouzenada, A. et al. Thermal properties of the 2D Klein-Gordon oscillator in a cosmic string space-time. *Theor. Math. Phys.***216**, 1055. https://doi.org/10.1134/S0040577923070115 (2023).
22. Hassanabadi, H. et al. The statistical properties of Klein-Gordon oscillator in noncommutative space. *J. Math. Phys.***55**, 033502. https://doi.org/10.1063/1.4866978 (2014).
23. Liang, M. L. & Yang, R. L. Three-dimensional Klein-Gordon oscillator in a background magnetic field in noncommutative phase space. *Int. J. Mod. Phys. A***27**, 1250047. https://doi.org/10.1142/S0217751X12500479 (2012).
24. Haouam, I. On the noncommutative geometry in quantum mechanics. *J. Phys. Stud.* **24**, 2002. https://doi.org/10.30970/jps.24.2002. (2020).
25. Madore J (2000) An introduction to noncommutative geometry. In: H. Gausterer, L. Pittner, H. Grosse, (eds) Geometry and Quantum Physics. Lecture Notes in Physics, vol 543. (Springer, Berlin, Heidelberg, 2000). https://doi.org/10.1007/3-540-46552-9_5
26. Carroll, S. M. et al. Noncommutative field theory and Lorentz violation. *Phys. Rev. Lett.***87**, 141601. https://doi.org/10.1103/PhysRevLett.87.141601 (2001).
27. Haouam, I. On the Fisk-Tait equation for spin-3/2 fermions interacting with an external magnetic field in NC space-time. *J. Phys. Stud.* **24**, 1801. https://doi.org/10.30970/jps.24.1801 (2020).
28. Martinetti, P. Beyond the standard model with NC geometry, strolling towards quantum gravity. *J. Phys.: Conf. Ser.* **634**, 012001. https://doi.org/10.1088/1742-6596/634/1/012001 (2015).
29. Seiberg, N. & Witten, E. String theory and noncommutative geometry. *J. High Energy Phys.***1999**, 032. https://doi.org/10.1088/1126-6708/1999/09/032 (1999).
30. Connes, A. et al. Noncommutative geometry and matrix theory. *J. High Energy Phys.***1998**, 003. https://doi.org/10.1088/1126-6708/1998/02/003 (1998).
31. Gingrich, D. M. Noncommutative geometry inspired black holes in higher dimensions at the LHC. *J. High. Energy. Phys.* **2010**, 22. https://doi.org/10.1007/jhep05(2010)022 (2010).
32. Gracia-Bondia, J. M. Notes on Quantum Gravity and Noncommutative Geometry: New Paths Towards Quantum Gravity (Springer, Berlin. *Heidelberg* https://doi.org/10.1007/978-3-642-11897-5_1 (2010).
33. Haouam, I. & Hassanabadi, H. Exact solution of (2+1)-d NC Pauli eq in a time-dependent background. *Int. J. Theor. Phys.* **61**, 215. https://doi.org/10.1007/s10773-022-05197-5 (2022).
34. Fring, A. et al. Strings from position-dependent noncommutativity. *J. Phys. A Math. Theor.***43**, 345401. https://doi.org/10.1088/1751-8113/43/34/345401 (2010).
35. Gomes, M. & Kupriyanov, V. G. Position-dependent noncommutativity in quantum mechanics. *Phys. Rev. D***79**, 125011. https://doi.org/10.1103/PhysRevD.79.125011 (2009).
36. Gouba, L. A comparative review of four formulations of noncommutative quantum mechanics. *Int. J. Mod. Phys. A***31**, 1630025. https://doi.org/10.1142/S0217751X16300258 (2016).
37. Haouam, I. Foldy-wouthuysen transformation of noncommutative Dirac equation in the presence of minimal uncertainty in momentum. *Few-Body Syst.***64**, 9. https://doi.org/10.1007/s00601-023-01790-4 (2023).
38. Haouam, I. Classical limit and Ehrenfest's theorem versus non-relativistic limit of noncommutative Dirac equation in the presence of minimal uncertainty in momentum. *Int. J. Theor. Phys.***62**189. https://doi.org/10.1007/s10773-023-05444-3 (2023).
39. Haouam, I. Two-dimensional Pauli equation in noncommutative phase-space. *Ukr. J. Phys.***66**, 771. https://doi.org/10.15407/ujpe66.9.771 (2021).
40. Chaichian, M. et al. Hydrogen atom spectrum and the Lamb shift in noncommutative QED. *Phys. Rev. Lett.***86**, 2716. https://doi.org/10.1103/PhysRevLett.86.2716 (2001).
41. Haouam, I. Dirac oscillator in dynamical noncommutative space. *Acta Polytech.***61**, 689. https://doi.org/10.14311/AP.2021.61.0689 (2021).
42. Haouam, I. & Alavi, S. A. Dynamical noncommutative graphene. *Int. J. Mod. Phys. A***37**, 2250054. https://doi.org/10.1142/S0217751X22500543 (2022).
43. Haouam, I. & Alavi, S. A. Landau problem in dynamical noncommutative space. *Ann. Phys.***469**, 169776. https://doi.org/10.1016/j.aop.2024.169776 (2024).
44. Haouam, I. Analytical solution of (2+1) dimensional Dirac eq in time-dependent NC phase-space. *Acta. Polytech.* **60**, 111. https://doi.org/10.14311/AP.2020.60.0111 (2020).
45. N'Dolo, E. E. Non-Hermitian 2D harmonic oscillator in NC phase-space. *Int. J. Geom. Methods Mod. Phys.* **21**, 2450085. https://doi.org/10.1142/S0219887824500853 (2024).
46. Lawson, L. M. Minimal and maximal lengths from position-dependent non-commutativity. *J. Phys. A, Math. Theor.***53**, 115303. https://doi.org/10.1088/1751-8121/ab7497 (2020).
47. Bagchi, B. & Fring, A. Minimal length in quantum mechanics and non-Hermitian Hamiltonian systems. *Phys. Lett. A***373**, 4307. https://doi.org/10.1016/j.physleta.2009.09.054 (2009).
48. Bender, C. M. Making sense of non-hermitian Hamiltonians. *Rep. Prog. Phys.***70**, 947 (2007).
49. Boumali, A. & Hassanabadi, H. The thermal properties of a 2D Dirac oscillator under an external MF. *Eur. Phys. J. Plus* **128**, 124. https://doi.org/10.1140/epjp/i2013-13124-y (2013).
50. Arfken, G. *Mathematical Methods for Physicists* 3rd edn, 327–338 (Academic Press, 1985).
51. Pacheco, M. H. et al. One-dimensional Dirac oscillator in a thermal bath. *Phys. Lett. A***311**, 93. https://doi.org/10.1016/S0375-9601(03)00467-5 (2003).
52. Boyacioglu, B. & Chatterjee, A. Dia- and paramagnetism and total susceptibility of GaAs quantum dots with Gaussian confinement. *Phys. E Low-Dimens. Syst. Nanostruct.***44**(9), 1826. https://doi.org/10.1016/j.physe.2012.05.001 (2012).
53. Bera, A., Ghosh, A. & Ghosh, M. Analyzing magnetic susceptibility of impurity doped quantum dots in presence of noise. *J. Magn. Magn. Mater.***484**, 391. https://doi.org/10.1016/j.jmmm.2019.04.005 (2019).
54. Arda, A. et al. Klein-Gordon and Dirac Equations with Thermodynamic Quantities. *Few-Body. Syst* **57**, 93. https://doi.org/10.1007/s00601-015-1031-7 (2016).
55. Boumali, A. One-dimensional thermal properties of the Kemmer oscillator. *Phys. Scr.***76**, 669. https://doi.org/10.1088/0031-8949/76/6/014 (2007).
56. Boumali, A. The one-dimensional thermal properties for the relativistic harmonic oscillators. *EJTP***12**, 121 (2015).

Acknowledgements
The author would like to thank the anonymous reviewers for their careful reading of the manuscript and for their insightful comments.

Author contributions
I, Haouam wrote the main manuscript text and prepared figures 1-15. He also reviewed the manuscript.

Funding
This research received no external funding.

Declarations

Competing interests
The authors declare no competing interests.

Additional information
Correspondence and requests for materials should be addressed to I.H.

Reprints and permissions information is available at www.nature.com/reprints.

Publisher's note Springer Nature remains neutral with regard to jurisdictional claims in published maps and institutional affiliations.